Contribution of Western Arabian Sea Tropical Cyclones to Rainfall in the Horn of Africa and Southern Arabian Peninsula

Pierre Camberlin, Omar Assowe Dabar, B. Pohl, M. Mohamed Waberi, Karl Hoarau, O. Planchon

JGR Atmospheres

RESEARCH ARTICLE
10.1029/2024JD041109

Contribution of Western Arabian Sea Tropical Cyclones to Rainfall in the Horn of Africa and Southern Arabian Peninsula

P. Camberlin[1], O. Assowe Dabar[2], B. Pohl[1], M. Mohamed Waberi[1,2], K. Hoarau[3], and O. Planchon[1]

[1]Centre de Recherches de Climatologie, UMR 6282 Biogéosciences, CNRS, Université de Bourgogne, Dijon, France, [2]Observatoire Régional de Recherche sur l'Environnement et le Climat (ORREC), Centre d'Etudes et de Recherche de Djibouti (CERD), Djibouti, Republic of Djibouti, [3]PLACES, CY Cergy Paris Université, Cergy, France

Key Points:

- An average 1.5 tropical cyclones occur annually in the Western Arabian Sea, 70% of them in September–December, the rest in May–June
- They strongly contribute (30%–60%) to rainfall over the northwestern Arabian Sea, the Gulf of Aden and their coastlines
- Their frequency sharply increased from 1990 to 2020, resulting in a 11% rise of their contribution to the Gulf of Aden precipitation

Correspondence to:
P. Camberlin,
camber@u-bourgogne.fr

Citation:
Camberlin, P., Assowe Dabar, O., Pohl, B., Mohamed Waberi, M., Hoarau, K., & Planchon, O. (2024). Contribution of western Arabian Sea tropical cyclones to rainfall in the Horn of Africa and southern Arabian Peninsula. *Journal of Geophysical Research: Atmospheres*, *129*, e2024JD041109. https://doi.org/10.1029/2024JD041109

Received 1 MAR 2024
Accepted 1 AUG 2024

Abstract The occurrence of tropical cyclones (TCs) in the Horn of Africa and nearby areas is for the first time examined to document their contribution to local rainfall and their trends over the period 1990–2020. An average 1.5 TC (of any intensity) per year was observed over the Western Arabian Sea, with two asymmetrical seasons, namely May–June (30% of cyclonic days) and September–December (70%). Case studies reveal that in many instances, TC-related rainfall extends beyond 500 km from the TC center, and that substantial rains occur one to 2 days after the lifecycle of the TC. Despite their rarity, in the otherwise arid to semi-arid context characteristic of the region, TCs contribute in both seasons to a very high percentage of total rainfall (up to 30%–60%) over the northwestern Arabian Sea, the Gulf of Aden and their coastlines. Over inland northern Somalia, contributions are much lower. TCs disproportionately contribute to some of the most intense daily falls, which are often higher than the mean annual rainfall. A strong increase in the number of TCs is found from 1990 to 2020, hence their enhanced contribution to local rainfall. This increase is associated with a warmer eastern/southern Arabian Sea, a decrease in vertical wind shear, and a strong increase in tropospheric moisture content.

Plain Language Summary The role played by tropical cyclones in local rainfall in the Horn of Africa and nearby areas is for the first time examined. An average 1.5 cyclones (of any intensity) per year is observed over the Western Arabian Sea. They occur in two different seasons: May–June (30% of cyclonic days) and September–December (70%). Despite their rarity, these cyclones affect a region which displays arid to semi-arid climates, hence they contribute to a very high percentage of total rainfall (30%–60%) over the northwestern Arabian Sea, the Gulf of Aden and their coastlines. Over inland northern Somalia, contributions are lower. Many of the most intense rainfall events are related to cyclones, with daily rainfall sometimes higher than the mean annual rainfall. There has been a strong increase in the number of cyclones from 1990 to 2020, and they contribute more to local rainfall. This increase is associated with a warmer Arabian Sea, a change in the wind flow and a higher moisture content.

1. Introduction

Tropical cyclones (TCs) develop over sufficiently warm off-equatorial oceanic regions, which are generally wet areas receiving well over 1,000 mm of precipitation per year. Although the Arabian Sea is not among the most active cyclonic basins, accounting, together with the Bay of Bengal, for only 4%–6% of the world's TCs (Neumann, 2017; Ramsay, 2017; V. K. Singh & Roxy, 2022), it stands out by its low mean annual rainfall (MAR), which does not exceed 500 mm in its northwestern half. Very few other arid regions, like northwestern Mexico (Breña-Naranjo et al., 2015; Fors, 1977) and Western Australia (Ng et al., 2014), similarly experience TCs. Although considered a very rare occurrence along the coasts of northern Somalia, Yemen, and to some extent Oman (Al-Manji et al., 2021; Pedgley, 1969), the recent past provided evidence of several high intensity systems, for example, the "very severe cyclonic storms" Gonu in 2007, Chapala and Megh in 2015, Mekunu and Luban in 2018. Their landfall in arid environments provides unusually high rainfall amounts in a short period of time, which have major short-term consequences (e.g., flash floods destroying infrastructure, settlements, claiming lives and killing livestock) as well as longer-term impacts, for instance on groundwater recharge (Abdalla & Al-Abri, 2011) and the dynamics of endangered tree species (Lvončík et al., 2020). In the late 2010s, the succession of several unusually wet seasons, in which TCs played a dominant role, induced the worst locust outbreak of the last decades in Southern Arabia and the Horn of Africa (Owuor & David McRae, 2022; Salih et al., 2020). In the

Republic of Djibouti alone, the desert locust infestation in 2019–2020 caused a loss of 5 million USD over crops and pastures. Even moderately strong tropical systems have large impacts because of the associated heavy rains. For instance, cyclonic storm Sagar brought 181 mm of rainfall in Djibouti-city on 2 days in May 2018, extensively flooding huge urban neighborhoods and schools, and destroying transportation and sanitation infrastructures (Cherel et al., 2020). The low income populations of the Horn of Africa, usually confronted to harsh climatic conditions related to recurrent droughts, are particularly vulnerable to such high intensity rainfall events, yet to the best of our knowledge there has never been any systematic study of how frequently TCs affect this part of the continent.

Over the Western Arabian Sea (WAS hereafter) and neighboring coastal areas (Yemen, Somalia, Djibouti), more generally, the average contribution of TCs to local rainfall is little known. Pedgley (1969) found that at Salalah (southern Oman), a quarter of the total rainfall from 1943 to 1967 was associated with cyclones. Jiang and Zipser (2010) and Prat and Nelson (2013) quantified the contribution of tropical storms to global precipitation from Tropical Rainfall Measurement Mission (TRMM) data. Over the period 1998–2006, it varied from 3% to 11% depending on the basins (Jiang & Zipser, 2010), and 5% for the North Indian Ocean basin which includes both the Bay of Bengal and the Arabian Sea. Comparable values were obtained by Prat and Nelson (2013) using 12 years of data from 1998 to 2009. Much higher contributions were found over localized areas such as the coasts of Baja California in Mexico (Breña-Naranjo et al., 2015) and northwest Australia (Ng et al., 2014), but they decrease significantly within the first 150 km from the coast (Prat & Nelson, 2013). Khouakhi et al. (2017) examined the contribution of TCs to rain-gauge precipitation amounts and found that they account for a large portion (35%–50%) of MAR in a few regions including northwestern Australia, southeastern China, the northern Philippines, and northwestern Mexico. However, their study did not document the Arabian Sea area. Prat and Nelson (2013) published a map covering the North Indian Ocean basin, but due to the small number of years, the TC-related rainfall contribution is relatively noisy over the WAS. Kabir et al. (2022) studied TC exposure in the North Indian Ocean. TC-associated rainfall is much higher around the Bay of Bengal sub-basin than over the Arabian Sea, partly due to the larger number of TCs making landfall around the Bay of Bengal (155 between 1989 and 2018, as compared to 30 around the Arabian Sea). Nevertheless, the latter have a high contribution to TRMM total rainfall along the southeastern coasts of Arabia, reaching 50% in parts of Oman (Kabir et al., 2022).

The objectives of the present study are to quantify the mean rainfall amount resulting from TCs in the WAS, Gulf of Aden and riverine countries (Somalia, Djibouti, Yemen), and their contribution to the total rainfall amounts, which have never been comprehensively analyzed before, since all previous studies on TC-induced precipitation were actually carried out at a much broader scale. Daily rainfall extremes associated with TCs will also be examined and compared to local absolute 24-hr maxima. Some case studies of TCs making landfall over the coasts of Somalia and Djibouti will also be presented in order to better comprehend the spatial distribution of rainfall during such events and its relationship to the storms size and track. A better knowledge of TCs in the region and their contribution to the local climatology is an important issue, because several studies point to a recent (Baburaj et al., 2020; Deshpande et al., 2021; Murakami et al., 2017; Priya et al., 2022; Tiwari et al., 2022; B. Wang et al., 2012) and forthcoming increase (Bell et al., 2020; Knutson et al., 2015; Murakami et al., 2013) in the frequency of Arabian Sea TCs. While Murakami et al. (2013) attributed the recent increase to anthropogenic climate change, more ambiguous results were obtained by S. Wang et al. (2023). Evan et al. (2021) found that a recent increase in storm intensity could have been driven by enhanced anthropogenic black carbon and sulfate emissions, resulting in a reduction of vertical wind shear, but this was challenged by B. Wang et al. (2012).

Besides documenting the patterns of TC-related rainfall over the north-eastern tip of Africa and adjacent regions, the present study analyses trends of TC-related and total rainfall over the last 20–30 years. Given the major changes found in TC occurrence in the last decades, a comparison is also made of the regional oceanic and atmospheric conditions which may have triggered these changes. Section 2 presents the cyclone and precipitation data used in the study. The TC and precipitation climatologies are depicted in Section 3.1, followed by the selected TC case studies (Section 3.2). The statistical analysis of mean rainfall amounts associated with TCs is then presented (Section 3.3), before an appraisal of TC-related rainfall trends since 1990 (Section 3.4) and the associated oceanic and atmospheric conditions (Section 3.5).

2. Data and Methods

2.1. Cyclone Tracks

Data on 3-hourly North Indian Ocean TC locations were extracted from the International Best Track Archive for Climate Stewardship (IBTrACS, Knapp et al., 2010, 2018) data set. All observations west of 75°E were retained. This is slightly further east than the WAS target area (33–65°, 0–22°N) because it is necessary to extract TC-related rainfall over a wide radius from the TC center. Given that some of the rainfall data are at daily time-scale, the successive locations of each cyclone are averaged over each 24-hr period. As discussed below, the wide radius which will be retained around the TC center accommodates the TC propagation within each day.

All TC categories were retained in the study, that is, including weak systems like tropical depressions or deep depressions (wind speeds between 17 and 34 knots). Substantial rains are sometimes associated with tropical depressions, which justifies the inclusion of these weaker systems. For instance, Arabian Sea tropical depression 02A, with weak maximum sustained winds (25 knots), which in 2008 made landfall in Yemen, caused widespread flooding, 180 deaths and 22,000 displaced people (Evan & Camargo, 2011). Some analyses will be separately carried out on the Very Severe Cyclonic Storms (VSCS hereafter), the third highest category used by the India Meteorological Department to classify North Indian Ocean TCs, and which is equivalent to the Hurricane category (winds of at least 64 knots). Hereafter, TC refers to all categories of disturbances, not just VSCS.

The study is restricted to the period from 1990 (2000 for some analyses) to 2020. Data for the pre-satellite era over the North Indian Ocean are not fully reliable due to a possible undercount of TCs (Deshpande et al., 2021; Evan & Camargo, 2011; K. Singh et al., 2020; Wahiduzzaman et al., 2022). Additionally, Kabir et al. (2022) and Tiwari et al. (2022) warned that TC records over the North Indian Ocean may not be fully complete prior to 1990 due to missing intensity records. Hoarau et al. (2012) re-analyzed TC data over the Northern Indian Ocean using the Dvorak (1984) method. They warned of a probable undercount of intense TCs during 1980–1989. From 1990 onwards, the agreement between North Indian Ocean TC track-data from the Indian Meteorological Department (IMD) and the Joint Typhoon Warning Center (JTWC) greatly improved (Evan & Camargo, 2011; Schreck et al., 2014), suggesting that working on this period is less uncertain.

2.2. Precipitation Data

Two daily gridded precipitation data sets based on satellite information calibrated with some ground data were used and complemented by rain-gauge data for northern Somalia and Djibouti. The gridded data sets were selected to document both land and oceanic areas, at a relatively high spatial resolution.

Precipitation Estimation from Remotely Sensed Information using Artificial Neural Networks–Climate Data Record (PERSIANN-CDR—Sorooshian et al., 2014) uses infrared (IR) satellite data as the main input, from which a neural network model is developed whose parameters are based on radar data. The resulting rainfall estimates are next calibrated using the monthly Global Precipitation Climatology Project data. The product is available from 1 January 1983 to the present, at 0.25° spatial resolution.

Integrated Multi-satellitE Retrievals for the Global Precipitation Measurement (IMERG, Huffman et al., 2019) is a gridded rainfall product with global coverage, based on NASA's precipitation algorithm, applied to data from the TRMM and the Global Precipitation Measurement (GPM) satellite missions. It covers the period from 2000 to the present day, at a high spatial (0.1°) and temporal (30 min) resolution. The input data include passive microwave (PMW) precipitation estimates, considered as more direct retrievals, calibrated to the combined radar-radiometer product from TRMM and GPM. An interpolation of the PMW estimates is performed by propagating them forward and backward in time using motion vectors. The resulting estimates are further combined to IR precipitation estimates, and a final bias adjustment to rain-gauge observations is made over land areas.

For both data sets, the region 3°S–22°N, 35–65°E, that is, the Greater Horn of Africa (GHA) and nearby regions, was extracted. The period retained is 1990–2020 (2000–2020 for IMERG) to take into account TC data reliability as exposed above. Note that, unless otherwise stated, the results obtained for PERSIANN and IMERG are qualitatively similar, hence will not be systematically duplicated. Below, IMERG is generally preferred to PERSIANN, because it slightly better agrees with rain-gauge data.

Daily rain-gauge data for 25 stations in Northern Somalia (mainly Somaliland and Puntland areas) were obtained from Somalia Water and Land Information Management (SWALIM), a project managed by FAO. The period

covered is 2005–2020, with data availability varying from 10 to 16 years. For the Republic of Djibouti, data from Djibouti-Airport station, with complete daily rainfall records between 2000 and 2020, were obtained from the National Meteorological Agency of Djibouti.

2.3. Methods for Quantifying TC-Associated Precipitation

Quantifying the contribution of TCs to rainfall requires defining to what distance of the TC center rainfall is considered as being related to the TC. Most studies consider a 500 km radius (e.g., Jiang & Zipser, 2010; Lavender & McBride, 2021; Prat & Nelson, 2013). This threshold is meant to be within the range of the outer edge of the TC cloud shield (550–600 km) (Englehart & Douglas, 2001; Kabir et al., 2022). Rather than blindly adopting the same threshold, mean daily rainfall was plotted as a function of distance to the TC center, for all TCs reported in the period 2000–2020 in the WAS area. Boxplots were constructed to derive the mean and median rainfall and its variability for 40 km bins (Section 3.3). These were compared to the climatology (obtained from all calendar days where TCs can be found over the WAS). From these plots an adapted threshold was defined at 750 km (see below), and all rainfall which fell within this distance from the TC center was considered as TC-related. Rainfall in the days immediately following the demise of each TC was also examined in order to find out whether part of it can be ascribed to remnants of the disturbance and/or lingering storm effects. This procedure was used to quantify TC-related rainfall for each disturbance, and to compute statistics for the period 2000–2020 based on the gridded PERSIANN and IMERG rainfall estimates, and the stations available in the years 2005–2020 in Northern Somalia and Djibouti.

The contribution of TC-related rainfall to total rainfall was computed. To document the part played by TCs on intense rainfall, days recording above 30 mm were extracted and the proportion which are TC-induced was computed. Maximum 24-hr rainfall at available rain-gauges was also examined to assess to which extent it relates to TC occurrence. These analyses were carried out separately on the two cyclonic seasons, that is, the pre-monsoon (May–June) and the post-monsoon (September–December).

Rainfall trends over the period 2000–2020 (extended to 1990–2020 for PERSIANN) were mapped for total rainfall, TC-related rainfall, non-TC related rainfall and the contribution of TC-related rainfall to total rainfall amounts. Mann-Kendall Tau statistics were computed to assess the statistical significance of the trends.

3. Results

3.1. Rainfall and TC Climatologies

The region around the northeastern tip of Africa is mostly an arid to semi-arid area, with less than 500 mm/year (Figure 1). MAR increases to the southeast, in the Central Indian Ocean, in the west over highland areas (Ethiopia, Kenya, Yemen), and along a narrow subcoastal belt stretching northward from Southern Kenya. The region covering most of South Arabia, the Gulf of Aden and neighboring areas is particularly arid (less than 200 mm/year), with no well-defined rainy season. Much of Somalia and its surroundings have two brief rainy seasons, in March–May and October–November. Due to the divergence of large-scale air flows, most of the region experiences dry boreal winters (December–February) and summers (June–September), the main exception being the Ethiopian highlands.

From 1990 to 2020, a total of 47 TCs crossed the WAS, with a mean life-time (within the region) of 4.6 days. The number of TCs gradually decreases from east to west (Figure 2), with tracks generally showing E-W or SE-NW directions. A minority of the TCs display more meridional tracks, with southerly propagations on rare occasions (e.g., TC Kyarr in 2019). Only about a third of these TCs made landfall over the continent, either on the coasts of Southern Arabia or on those of Somalia, with a few additional TCs which approached close to the coasts or crossed Socotra island. A small proportion of these disturbances belong to the VSCS category. On average, only 1.1 days.year^{-1} record a VSCS, as compared to 7.1 days.year^{-1} for all TC categories.

TCs reaching or developing over the WAS are found in two distinct seasons (Figure 2), which correspond to the pre-monsoon season (May–June) and post-monsoon season (September–December, clearly peaking in October–November). During the monsoon season (boreal summer), the strong wind shear between the low-level westerlies and the upper-tropospheric Tropical Easterly Jet, as well as the lower sea surface temperature (SST) over parts of the WAS, disable the development of TCs (Baburaj et al., 2020; Evan & Camargo, 2011; Gray, 1968). TCs are much less frequent in May–June (MJ) than in September–December (SOND). The latter season makes up about

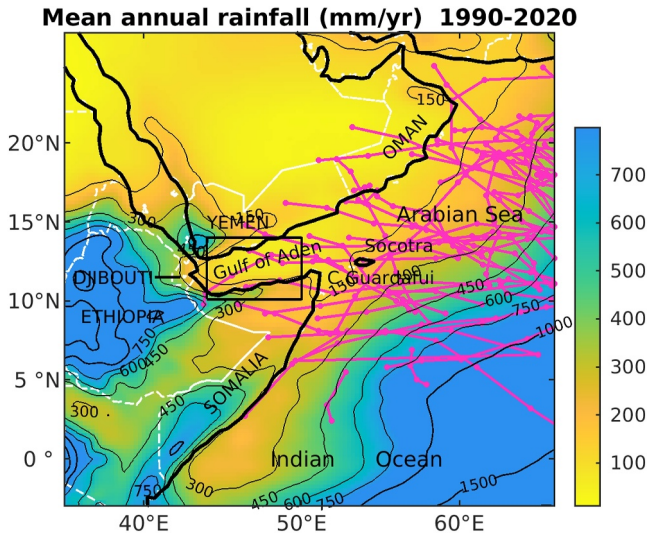

Figure 1. Location map, with shadings representing mean annual rainfall (PERSIANN data, 1990–2020, in mm) and pink lines tropical cyclone tracks (same period). The box shows the area over which the Gulf of Aden rainfall index is computed (Section 3.4).

two thirds of the number of TCs, and 70% of the cyclonic days. This is specific to the WAS: for the Arabian Sea as a whole the number of TCs is approximately the same in the two seasons (Evan & Camargo, 2011), with some decadal variations (Al-Manji et al., 2021). The smaller number of pre-monsoon TCs in the western part of the Arabian Sea compared to post-monsoon has rarely been highlighted (Ray-Choudhuri et al., 1959), though it is obvious in V. K. Singh and Roxy (2022, their Figure 3). There is no current explanation for this difference, but it is not related to SST, which are higher in the pre- than in the post-monsoon seasons. Dynamical conditions could be more conducive to a westward motion of the TCs initiated over the eastern Arabian Sea. The predominantly east-west tracks of many of the post-monsoon TCs is shown on Figure 2a. May–June tracks are slightly more uneven, and few of them make landfall over northeastern Africa or southern Arabia.

Large interannual variations are found in the number of TC days (Figure 2c). In some years, no TCs are recorded in the WAS. There has been a clear and strong positive trend in the number of TC days in the period 1990–2020 (+0.34 per year, significant at $p < 0.01$), corroborating Deshpande et al. (2021). Pettitt's test, a widely used rank-based non-parametric test for change-point detection (Pettitt, 1979), indicates a significant upward increase ($p < 0.01$) after 2009. In the first sub-period (1990–2009), there was an average of 3.9 TC days/year in the WAS, rising to 13 days/year between 2010 and 2020. Statistics for WSCS are less robust, given the rare occurrence of disturbances in this category. While these storms were exceptional between 1990 and 2009, they became much more common from 2010, with each of the last 3 years (2018, 2019, and 2020) recording VSCS.

3.2. Case-Studies

Four case studies of TCs which made landfall over the northeastern tip of Africa have been selected, to document the relationship between the tracks of these systems and the rainfall distribution. They are ordered here by increasing intensity.

3.2.1. Deep Depression ARB01/2013 (November 2013)

This disturbance was first identified as a low pressure center on 6 November 2013 near 6°N, 65°E (Figure 3), then classified by the IMD as a tropical depression on 8 November 2013, while located 680 km east of Ras Binnah on the northeastern Somalian coast, moving westward. It slightly intensified on 9 November, with 3-mn sustained winds of 55 km/hr, developed an eye feature, and was classified as a deep depression. It made landfall on 10 November at 8°30′N, north of Eyl in Puntland, northern Somalia. A large area of active convection was associated with the TC. Very high daily point rainfall estimates were obtained by IMERG along the track, from 199 mm to an unreliable 1,196 mm on 9 November near the coast (Figure 3, bottom), in conjunction with very low cloud top temperatures (−70 to −75°C, not shown). As the TC made landfall, very high rainfall estimates were still shown on 11 and 12 November over a large area covering northern Somalia. On 13 and 14 November, while the TC is no longer singularized, scattered but significant convective rains occurred from Djibouti to Central Somalia.

Rain-gauge data (Figure 4) show that coastal rains associated with the disturbance started on 8 November, but the bulk of the rains fell on 11 November in arid Puntland (20–100 mm, and a peak of 139 mm at Eyl). The rains shifted westward on 12 November, with substantial rains (40–50 mm) still found on 13 November in western Somaliland. The accumulated rainfall during the TC lifetime (within 750 km of the TC center, see Section 3.3 for justification) generally exceeds 100 mm in the east, and is more contrasted further west (Figure 4). However, if one adds the following 2 days (Figure 4, bottom right panel), rainfall amounts ranging from 49 to 144 mm are found in the inland part of western Somaliland. The coastal town of Berbera (55-year MAR: 50 mm) even recorded 195 mm during this period. In Somalia, TC ARB01/2013 caused the death of 162 people, about 100,000 livestock losses and the destruction of over 1,000 houses (IFRC, 2013).

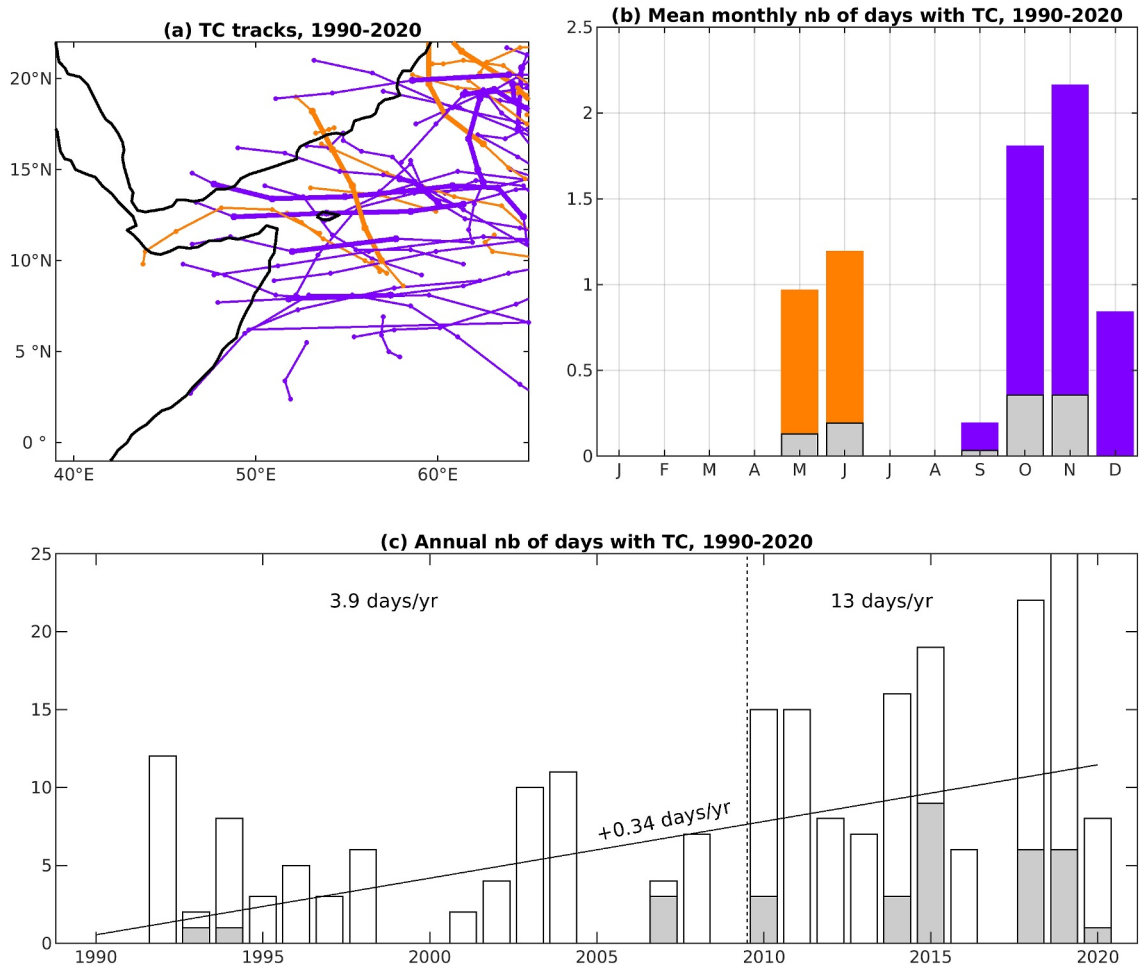

Figure 2. Tropical cyclone (TC) tracks and TC statistics for the Western Arabian Sea, 1990–2020. Orange colors refer to the May–June season, purple colors to the September–December season. Gray bars in panels (b) and (c) stand for Very Severe Cyclonic Storms, which are identified by bold lines in panel (a). In panel (c), white bars show the yearly total of TC days (TC center located west of 65°E), with the linear trend computed as Sen's slope. The vertical dashed line is the breaking point according to Pettitt's test ($p < 0.01$), with the mean number of TC days for the two sub-periods in the top part of the panel.

3.2.2. Cyclonic Storm Sagar (May 2018)

According to the JTWC, this system began as a tropical depression on 15 May south of Socotra. It was named Sagar after it reached the tropical storm stage (35 knots) near the entrance to the Gulf of Aden on 16 May. The rains recorded off the eastern coast of Somalia on 16–18 May (Figure 5, top left panel) were mainly due to convective cells developing in the cloud bands at the southern edge of Sagar. Proceeding toward the west-southwest, the storm gradually intensified to become a VSCS (65 knots) on 18 May. The Visible Infrared Imaging Radiometer Suite image from 10:28 UTC in the visible spectrum indicates that Sagar was a small diameter cyclone. On 19 May, downgraded to a severe cyclonic storm (60 knots), Sagar made landfall west of Berbera, Somaliland. The slow movement of the system and very cold cloud tops (−70°C to −80°C on Meteosat-8 images) explain the heavy rains over Somalia and Djibouti from 18 to 20 May (Figure 5, bottom panels). Substantial rains were also found on the following 2 days in eastern Ethiopia, associated with the overall atmospheric instability and Sagar remnants, causing landslides and destructive flash floods in the Sitti area. Wadi Ambouli, which crosses Djibouti-city, overflowed and caused heavy damages. Around 20,000 people were affected in the Republic of Djibouti. Damage to transport infrastructure amounted to approximately 1.9 billion Djiboutian francs (US$10 million), with a similar figure for the sanitation system (Cherel et al., 2020). At least 53 victims were numbered in northern Somalia, particularly in western Somaliland, herds were swept away, and many boats were destroyed in the ports of Puntland.

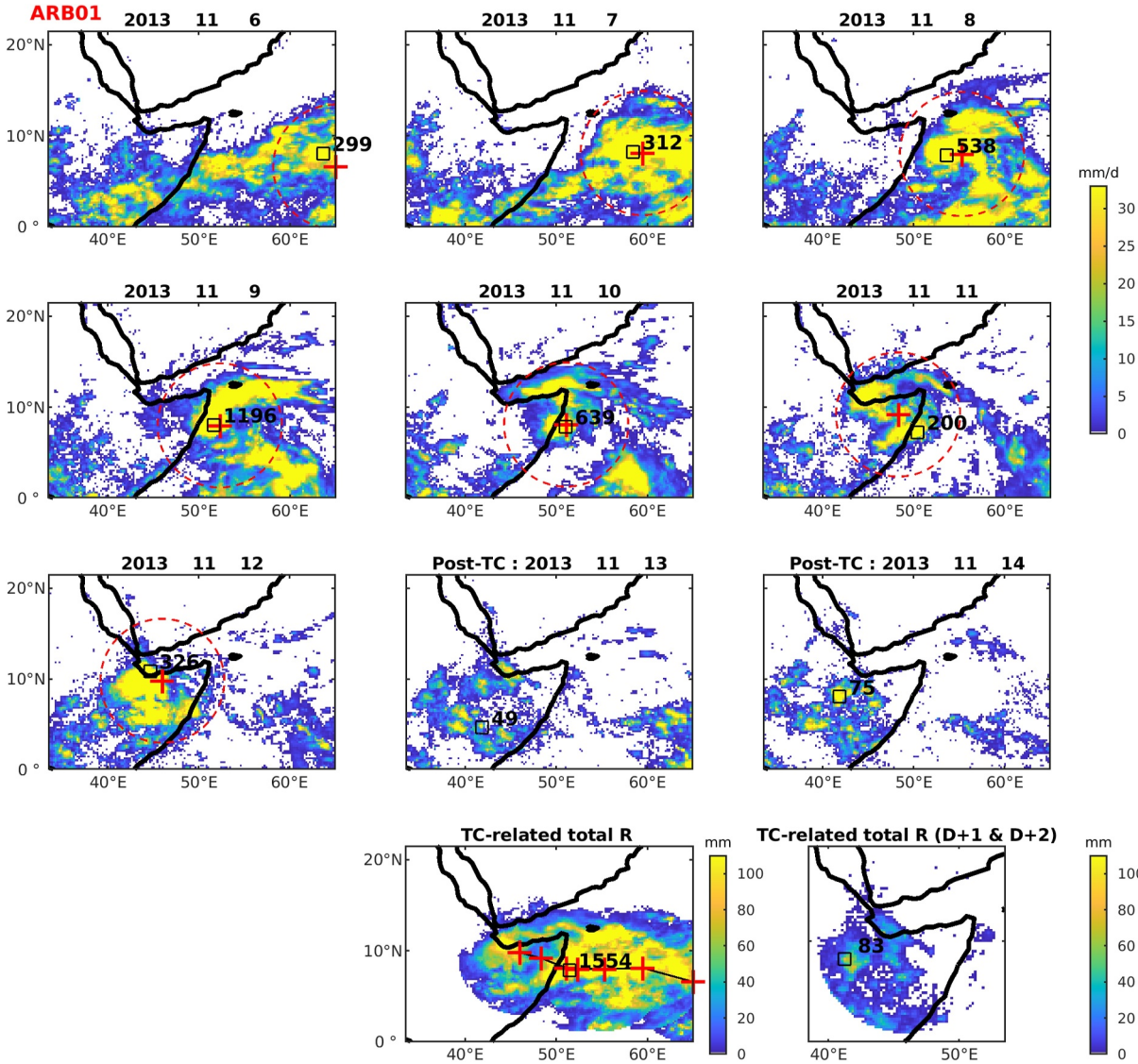

Figure 3. IMERG daily rainfall during the lifetime of deep depression ARB01/2013 and in the two following days ("post-tropical cyclone [TC]"). Red crosses: location of the TC center. Dashed circles: 750 km radius from the center (see justification in Section 3.3). Black squares: maximum rainfall amount within 750 km. Bottom panels: accumulated rainfall amount associated with the TC (within 750 km of its center) during its lifetime (left) and in the two following days (from the last known TC position, right panel).

3.2.3. VSCS Gati (November 2020)

Gati is a VSCS which showed an explosive intensification from a low pressure area located in the central Arabian Sea on 20 November 2020. Moving westwards (Figure 6), it made landfall near Hafun in northeastern Somalia on 22 November as a VSCS. Gati quickly weakened as it crossed land, with a last warning issued on 23 November over the Gulf of Aden. It resulted in maximum daily rainfall exceeding 100–200 mm every day from 20 to 23 November over the WAS, and in northeastern Somalia (Figure 7) several stations recorded daily rains over 70 mm on 22 and 23 November (e.g., at the hyper-arid station of Bosaso, 128 mm on 23 November, i.e., 780% of the 51-year MAR). Rainfall was lower further west, though an IMERG estimate of 180 mm is still noted in the Gulf of Aden on 24 November, and 65 mm recorded at Berbera on 25 November. Weaker rains were observed in Djibouti, but remnants of the storm brought heavy local rains on 25 and 26 November in eastern Ethiopia. Forty-two thousand people were displaced in Bari region, Puntland, Northeastern Somalia, with extensive damages due to flash floods, coastal submersion and winds (OCHA Somalia, 2020).

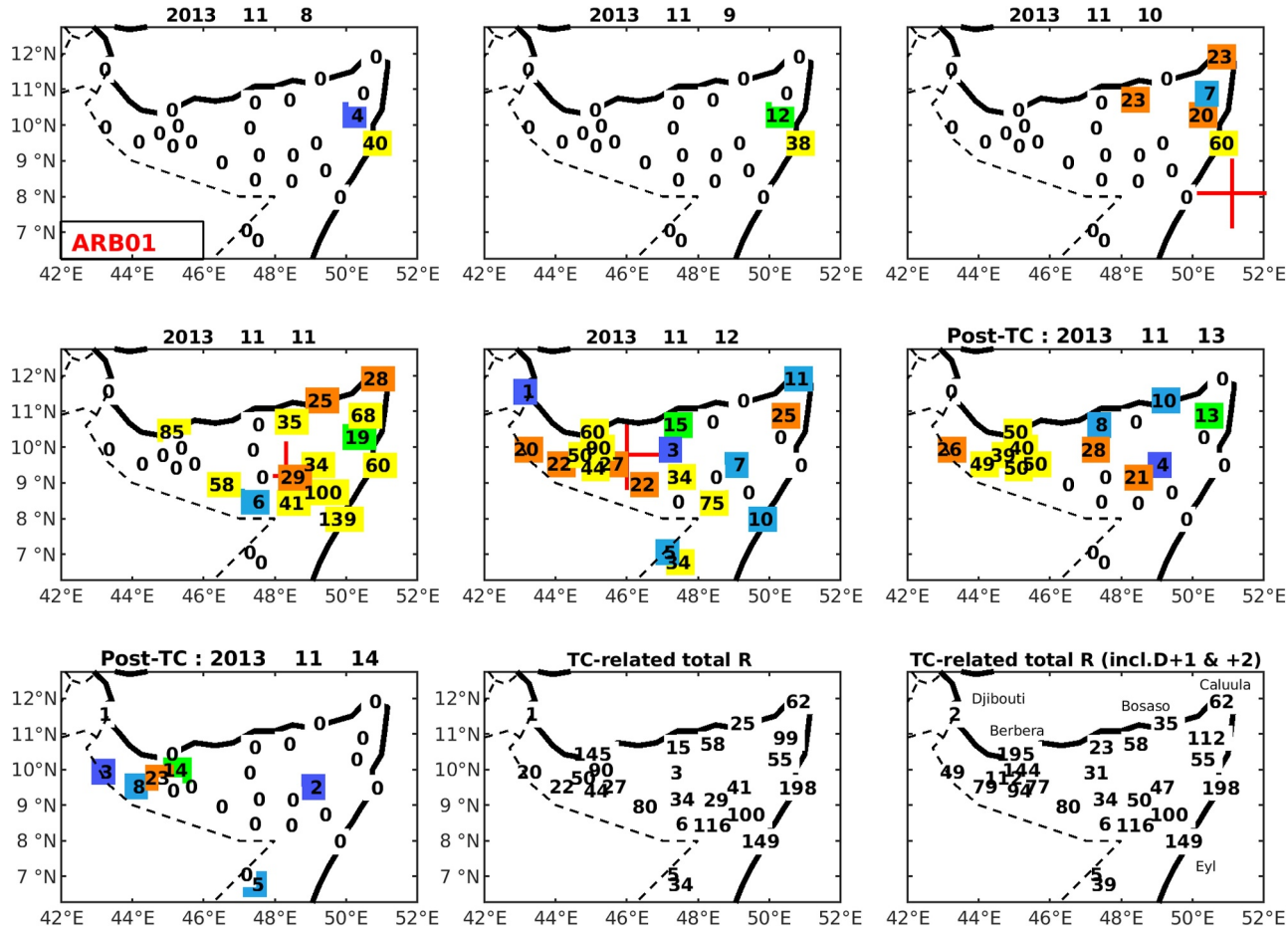

Figure 4. Daily rainfall over Northern Somalia and Djibouti during the lifetime of deep depression ARB01/2013 and in the two following days ("post-tropical cyclone [TC]"). Bottom panels show the accumulated rainfall amount associated with the TC (within 750 km of its center) during its lifetime (left) and including the two following days (right panel).

Although Gati had a trajectory roughly similar to that of Sagar, the heavy rains were felt more in the eastern than in the western part of its track. A detailed meteorological analysis is again out of scope, but the early landfall of Gati explained its fast weakening, hence the weaker rains in Western Somaliland and Djibouti. The more curvilinear path of Sagar, over the very warm Gulf of Aden (XBT soundings indicated that water temperature exceeded 27°C up to a depth of at least 29 m, not shown), provided a considerable heat flux which was sufficient to feed Sagar, despite its relatively slow motion.

3.2.4. VSCS 12A (October 1972)

Although rainfall maps are not available for this disturbance, since it predates the satellite era, it is an interesting case typical of the probable underreporting of some TC-related rainfall in the region, in this case due to incomplete TC tracks before 1982. Storm 12A originated from the southern Arabian Sea, moving northwestward to cross Socotra Island. It was classified as a VSCS (64–82 knots) just before its landfall over Socotra, then continued westwards while weakening. According to IBTrACS, this storm was last located at 12.2°N, 50.8°E, that is, 20 km north of Caluula, near Cape Guardafui, on 25 October 12:00 (with perfect agreement between the three IBTrACS sources). Yet the October 1972 monthly weather report in Djibouti (Résumé Mensuel du Temps, 1972) indicated that the storm, after entering the Gulf of Aden on 25 October at a speed of 5–6 knots, further penetrated westward with increased velocity (25–30 knots) and reached Djibouti in the morning of 27 October. Wind gusts of 36 knots were reported at Djibouti-Airport, 45 knots at Arta 40 km westwards. The track of this TC, along the Gulf of Aden, is therefore closer to Sagar in 2018 than Gati or ARB01. The relatively small size of the tropical systems which enter the Gulf of Aden, like storm 12A, may, before the satellite era, have resulted in their underreporting.

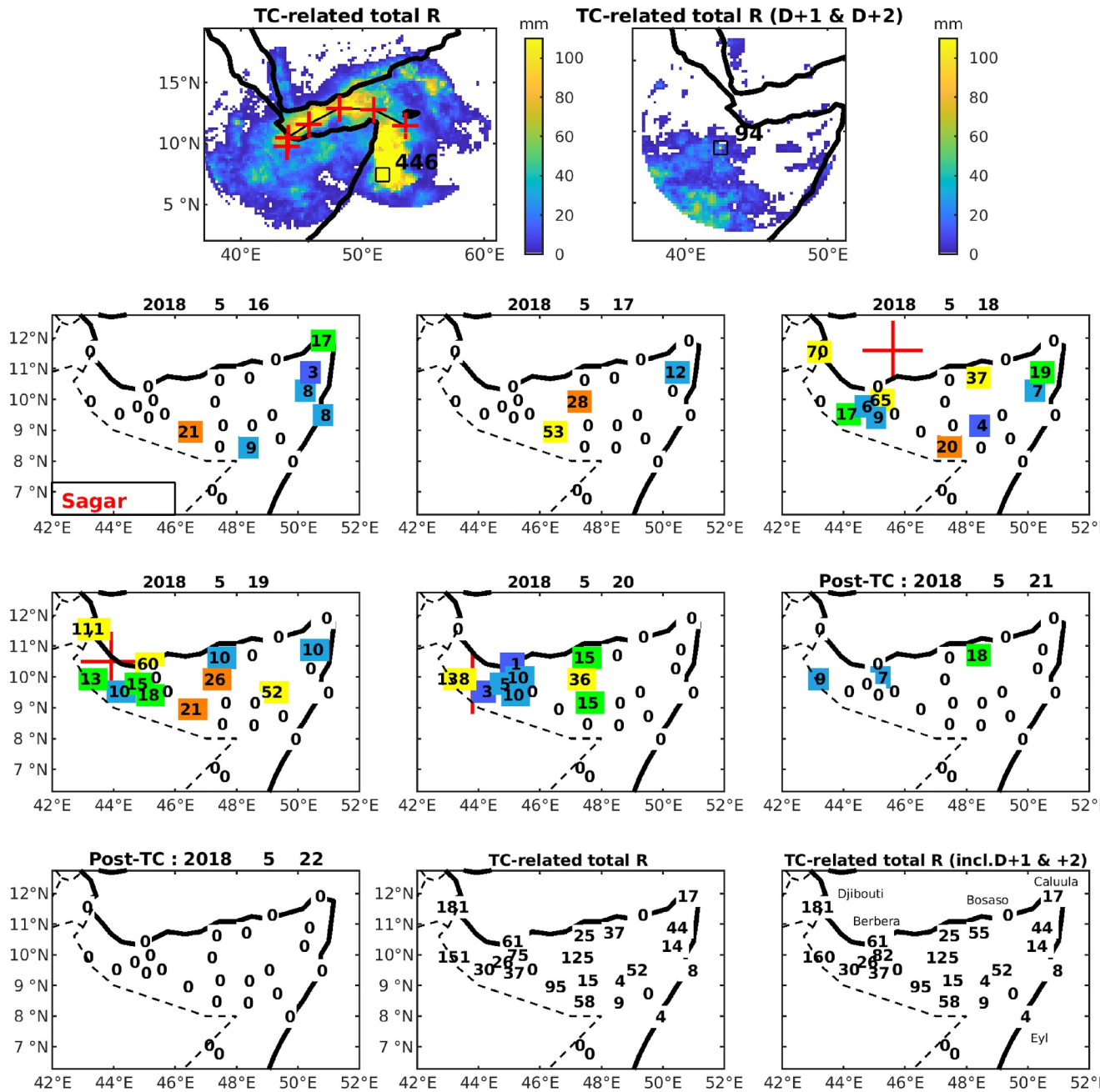

Figure 5. Rainfall associated with tropical cyclone (TC) Sagar. Top panels: accumulated IMERG rainfall during Sagar lifetime (15–20 May, top left) and in the two following days (21–22 May, top right). Red crosses show the track of the TC center. Black squares indicate the maximum accumulated rainfall amount (mm) within the 750 kms of the center. Bottom panels: daily rainfall over Northern Somalia and Djibouti and in the two following days ("post-TC").

Exceptionally high rains fell in the Djibouti area (201 mm at Djibouti-Airport on 27 October, 118% of the MAR), over the Gouda mountains (at Randa, 133 mm on the same day, 94 mm on 28 October) and at the usually very dry northern coastal station of Obock (105 mm on 27 and 28 October, compared to a MAR of only 73 mm). Rainfall quickly decreased further west (Dikhil: 2 mm, As Eyla: no rain). There is no daily data available from the northern coast of Somalia, while heavy rains fell further south in Central Somalia, but unlikely to be directly TC-related. The Northern Somalia Highlands, though close to the Gulf of Aden, reported only little rainfall (Hargeysa 6 mm on 28 and 29 October 1972), suggesting that the storm was of moderate size at this stage. There is only scanty information to assess the human losses and damages resulting from the storm. In Djibouti 60 people were reported

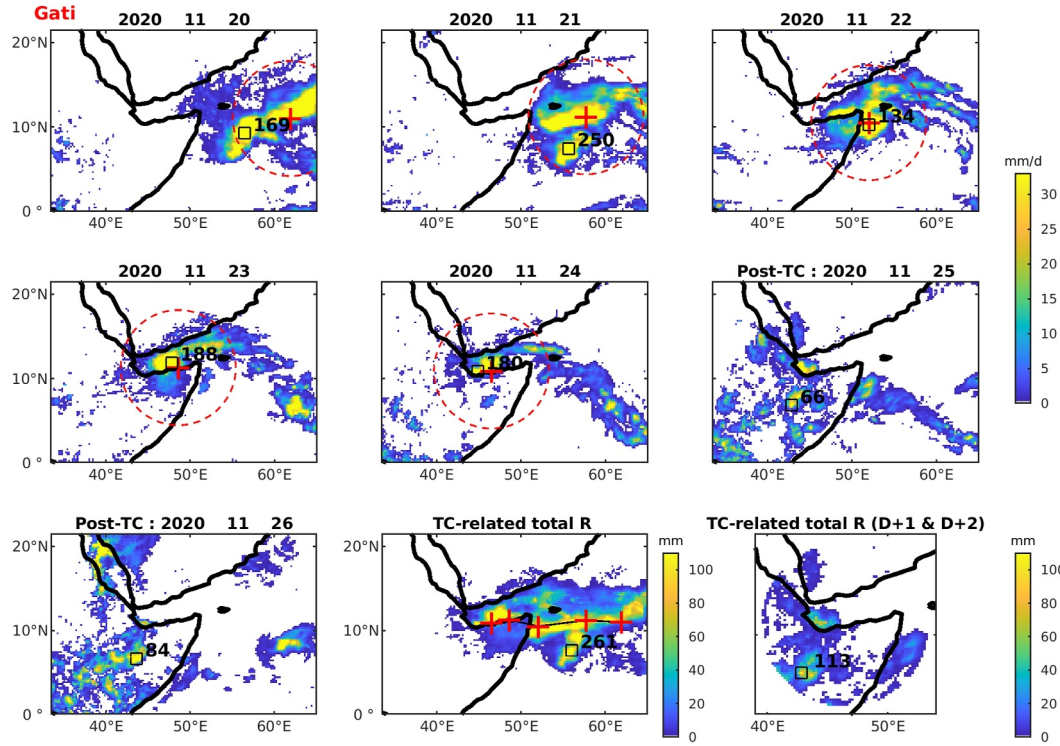

Figure 6. Same as Figure 3 but for Very Severe Cyclonic Storm Gati.

dead and 5,000 homeless. A third of the coastal palm groves in northeastern Somalia were destroyed by the storm, with long-lasting effects on springs due to landslides (Chazée, 2017).

Overall, several inferences can be made from these four case studies. First, although defining the exact zone of TC-related rainfall is uneasy, it is clear (e.g., Figure 3) that on several days this area extends beyond 500 km from the TC center. Second, in the 2 days following the reported termination date of the system, substantial rainfall, especially over land where the disturbance does not meet all the criteria to qualify as a tropical storm, is associated with remnants of the TC. Lastly, intense rainfall, with little relationship to the storm category, can be observed at arid locations. For instance, in northeastern Somalia, rainfall from deep depression ARB01/2013 (35–198 mm) often equals or exceeds MAR, which is as little as 15–200 mm. Over the ocean, even higher but highly localized rainfall amounts are found in IMERG.

3.3. Statistics of Rainfall Associated With TC Occurrence

This section aims to produce a statistical analysis of TC-related rainfall, over the period 2000–2020 for which cyclone data are very reliable and different sources of rainfall data are available. Rainfall on TC-days is plotted as a function of the distance to the TC center, for PERSIANN and IMERG (Figure 8). Both plots clearly show an exponential decay from the center. However, close to the center, rainfall is more intense in IMERG (83 mm at 0–20 km) than in PERSIANN (41 mm). This is partly due to the higher spatial resolution of IMERG, which better resolves very intense but highly localized downpours, and to the algorithm and input data used to estimating rainfall, which include microwave and radar data in IMERG. When screening for VSCS only (turquoise lines on Figure 9), even higher rainfall is noted close to the TC center. Gaona et al. (2018) showed the added value of IMERG in depicting rainfall intensities close to the TC center.

Visual examination of Figure 8 shows that after a strong decrease of rainfall amounts with increasing distance, the slope markedly reduces beyond 400–500 km, before gradually flattening out at roughly 600 km for IMERG and 700 km for PERSIANN. The boxplot height is smallest around 750 km in PERSIANN, and it is around this distance that the rainfall on TC-days becomes close to the climatology (black thick line on Figure 8). We therefore retain 750 km as a conservative threshold below which rainfall is considered as TC-related (and referred to as such

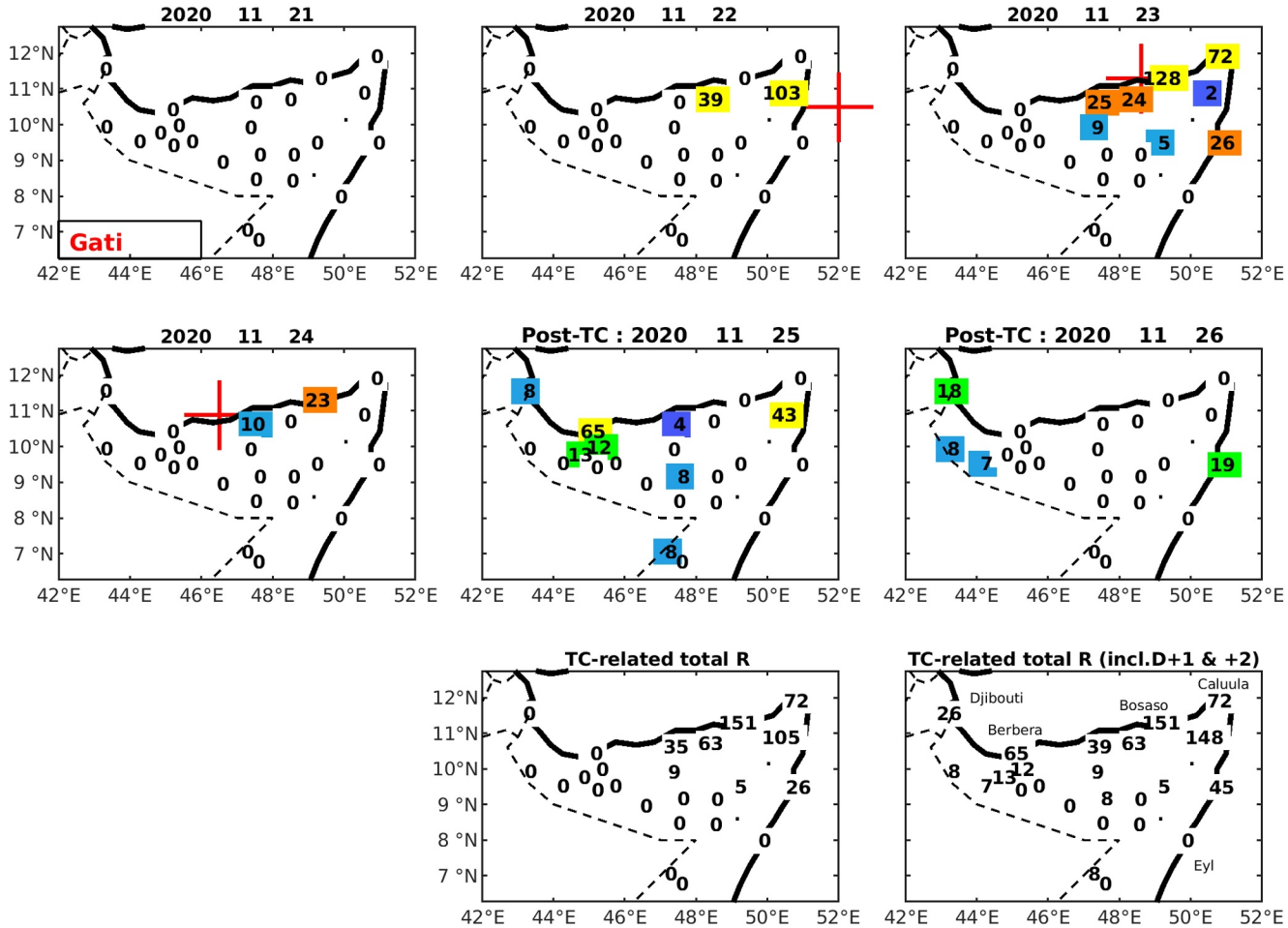

Figure 7. Same as Figure 4 but for Very Severe Cyclonic Storm Gati.

hereafter). This distance is greater than in most previous studies (500 km), but it is justified by the fact that the daily time-scale used in this study involves some propagation of the TC in a 24-hr period. Additionally, a cursory look at individual cyclones confirmed that a 500 km radius would exclude, in some cases, areas of convective activity which are clearly part of the disturbance (also see the above case studies). Note that for VSCS only, the drop to very low rainfall occurs at a slightly shorter distance, despite the much higher core intensities, suggesting more compact disturbances.

As suggested by the case-studies, TC-related rainfall does not necessarily stop as soon as the TC is no longer defined. Figure 8 shows rainfall one (panel c) and 2 days (panel d) after the TC lifecycle. The reference point for distance computation is that of the last known position of the TC center. On day +1, heavy rains (median of 21 mm/day) are still found within 20 km of the last known TC location. Between 40 and 400 km, although the elongated boxplots denote a diversity of patterns, substantial rains (medians from 9 to 19 mm/day, well above the climatology) reflect active remnants of the storm. On day +2, rainfall markedly decreases, but mean rainfall above 5 mm/day (again with a high dispersion, but well above the climatology) are found up to 600 km, with a median peaking at 8 mm at 280 km because of the shift of the storm remnants. This suggests that post-TC rainfall cannot be neglected. Hence, in the following, TC-related rainfall will be considered as the accumulated rainfall during the entire TC lifetime plus the following 2 days. Rainfall on day +3 is lower (median below 4 mm whatever the distance, not shown).

Mean rainfall on TC days and non-TC days is plotted for MJ and SOND (Figure 9). TCs bring substantial rains in the northwestern Arabian Sea, an otherwise relatively dry area in both seasons. Over the sea around Socotra and further to the north-east, intensities between 4 and 10 mm/day are recorded on TC days, while mean rainfall on

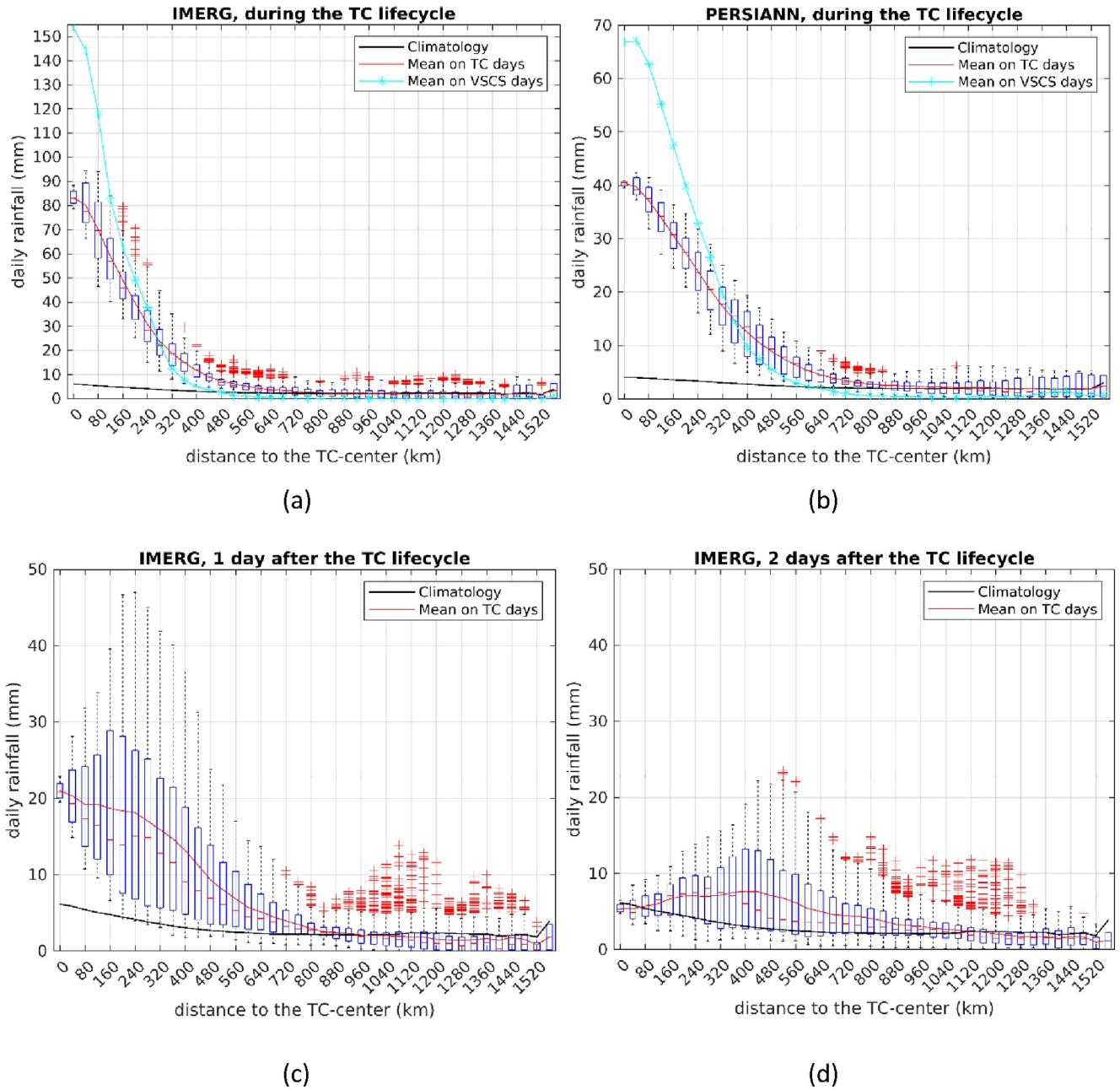

Figure 8. Boxplots of mean daily rainfall over the Western Arabian Sea (WAS), as a function of the distance to the tropical cyclone (TC) center. Top row: rainfall on TC-days, using IMERG (a) and PERSIANN (b) data for 2000–2020. Bottom row: IMERG rainfall a day (c) and 2 days (d) after the end of the TC lifecycle (the TC center refers to its last known location). The spread of the boxplots refers to spatial variations (i.e., in the mean rainfall among the pixels located in each distance bin). Black lines: 21-year climatology for the calendar days on which TCs occur. Red lines: mean rainfall for TCs. Turquoise lines (panels (a) and (b)): mean rainfall for Very Severe Cyclonic Storm (VSCS) only. Note the different vertical scales.

other days of the same seasons is generally below 1.5 mm/day. The patterns are quite similar for the two seasons, although noisier for MJ because TCs are less frequent. Near and along the coasts of northern Somalia, southern Yemen, southern Oman and in the Gulf of Aden, TC-related intensities are lower but in a context of even more arid conditions (<0.5 mm/day on non-TC days). This mostly reflects the smaller number of TCs reaching these areas. Over a broad area covering the northwestern Arabian Sea and nearby regions, the mean rainfall intensity is statistically higher (*t*-test, $p < 0.05$) on TC-days than during the same calendar days for years with no TCs (i.e., same day climatology: Figures 9b and 9d). Interestingly, some significant rainfall anomalies are also found

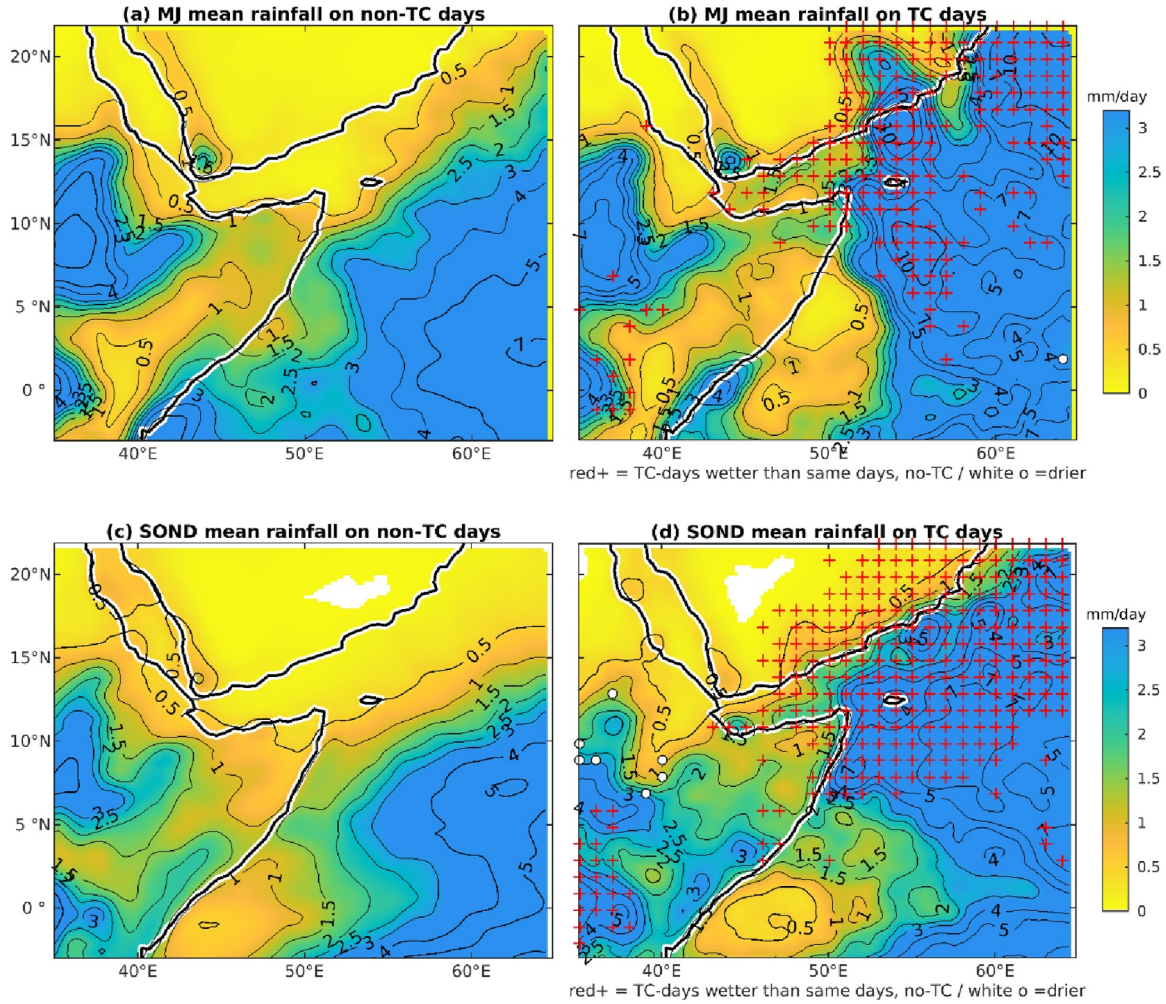

Figure 9. Rainfall (mm/day) on non-tropical cyclone (TC) days (left panels) and TC days (right panels) for May–June (a, b) and September–December (c, d), based on IMERG data (2000–2020). Red plus signs (white circles) indicate grid-points where rainfall on TC-days is significantly higher (lower) ($p < 0.05$) than that recorded on the same calendar days but with no-TC.

remotely from the WAS. Over central Ethiopia, localized drier than normal conditions (white circles) are found in SOND when a TC occurs in the WAS. By contrast, more rains than normal occur over Western Kenya (36–38°E, 2°S–5°N) in both seasons. This points to the distant effect of TCs, which will not be addressed here, but was already discussed for Southern Hemisphere cyclones (Finney et al., 2020; Kebacho, 2022; Shanko & Camberlin, 1998).

TC-related rainfall makes a very high contribution to climatological seasonal rainfall over the Arabian Sea northeast of Cape Guardafui (Figure 10). Over the northwestern Arabian Sea and Gulf of Aden, contributions reach 30%–50% of the seasonal mean along a belt running from the Gulf of Aden to Socotra island and the Yemen and Oman coasts. Contributions are more variable in MJ than SOND due to the small number of disturbances and their haphazard tracks. Values locally exceed 60% near the coasts, including inland southern Arabia near the border between Oman and Yemen. High contributions are also found at the northeastern tip of Somalia (30%–50%), quickly decreasing inland. On an annual basis (not shown), contributions exceed 30%, and even more than 50% over some areas according to PERSIANN. These values are quite remarkable given the relatively low occurrence of TCs in this basin. They are higher than those published in Prat and Nelson (2013) for the Arabian Sea, for several reasons like the different data set they used (TRMM), methodology, and their period of study (1998–2009) which does not include the recent very active years. These are among the highest values in the world. Among the cyclonic regions examined by Khouakhi et al. (2017), such high contributions are reached over only a

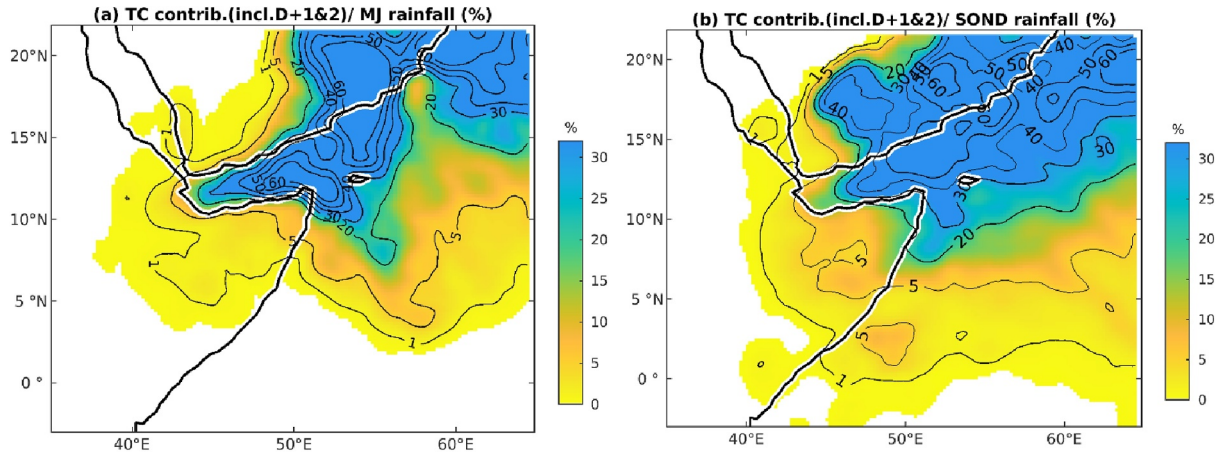

Figure 10. Percentage contribution of tropical cyclone (TC)-related rainfall to mean seasonal rainfall (IMERG data, 2000–2020), for May–June (MJ) (a) and September–December (SOND) (b). TC-related rainfall refers to rainfall within 750 km of the TC center, during its lifetime or in the next 2 days.

few coastal areas in the world, like northwestern Australia, Baja California, the northern Philippines and Hainan island in China, although their study did not consider oceanic areas.

Rain-gauge records confirm that over Northern Somalia the contribution of TC-related rainfall is often moderate, though it strongly increases along the coasts (Figure 11). In MJ (Figure 11a), it is below 10% inland, but much higher along the shores of the Gulf of Aden, in agreement with the higher contributions found over the sea in IMERG. In the western part of the Gulf, a high value (53%) is obtained at Djibouti, much higher than IMERG (10%). In agreement with IMERG, and with the exception of the Gulf of Aden, SOND contributions (Figure 11b) are generally higher than in MJ, due to a larger number of TCs. A broad east to west decrease is noted, which highlights the dominant westward tracks (Figure 2). However, arid stations along the Gulf of Aden get SOND contributions as high as 46% (Bosaso) and 47% (Berbera). Given the small number of TCs making landfall over the GHA, these are exceptionally high contributions.

The importance of TCs on rainfall is further underlined by focusing on intense rainfall events. Rain days recording more than 30 mm (IMERG data) are examined to find out how much TCs were contributing to these events. Over most of the Horn of Africa, the northern Arabian Sea, and moreover the southern Arabian Peninsula, the number of intense rainfall days is small (frequency <1%, i.e., less than 0.6 day.year^{-1} in MJ and 1.2 in SOND, not shown), but rain days above this threshold account for a significant to very high proportion of annual rainfall amounts (15%–40% over the GHA, 40%–50% over the Gulf of Aden, 50%–75% over the WAS). Conspicuously, a large share of these days (>40%, Figures 11e and 11f) is brought by TCs in the northwestern Arabian Sea and the Gulf of Aden, and in northeastern Somalia in SOND. This share even exceeds 60% over a belt extending from NE to SW along and offshore the Arabian Coast.

Rain-gauge data for northern Somalia and Djibouti confirm that in SOND at many stations the highest 24-hr rainfall is attributed to a TC (Figure 11d). In general, the maximum TC-related 24-hr rainfall is over 50 mm in this season, reaching values beyond 100 mm in most of the eastern stations. This is broadly in line with IMERG values. In MJ (Figure 11c), the highest TC-related 24-hr rainfall amounts are lower over the continent, and clearly more patchy (over the sea as well) as a result of fewer TCs. Interestingly, high values are nevertheless obtained in the north-west (60 mm at Berbera, 111 mm at Djibouti and 138 mm at Borama). Very intense rains are also associated with TC landfall over Oman (in Salalah for example, the absolute maximum rainfall measured during 1990–2020, 238.8 mm, was associated with the passage of cyclone Mekunu on 25 May 2018), but TC occurrence in this country is more thoroughly discussed in Al-Manji et al. (2021) and Pedgley (1969). Though IMERG also shows high values in the Gulf of Aden itself, near the coast satellite estimates are often lower than the observed contributions, because occasional very heavy precipitation along the coast are not always adequately resolved by the gridded products. Such an underestimation of coastal intense precipitation in gridded products is found in other parts of Africa (e.g., the Guinea Coast; Kpanou et al., 2021).

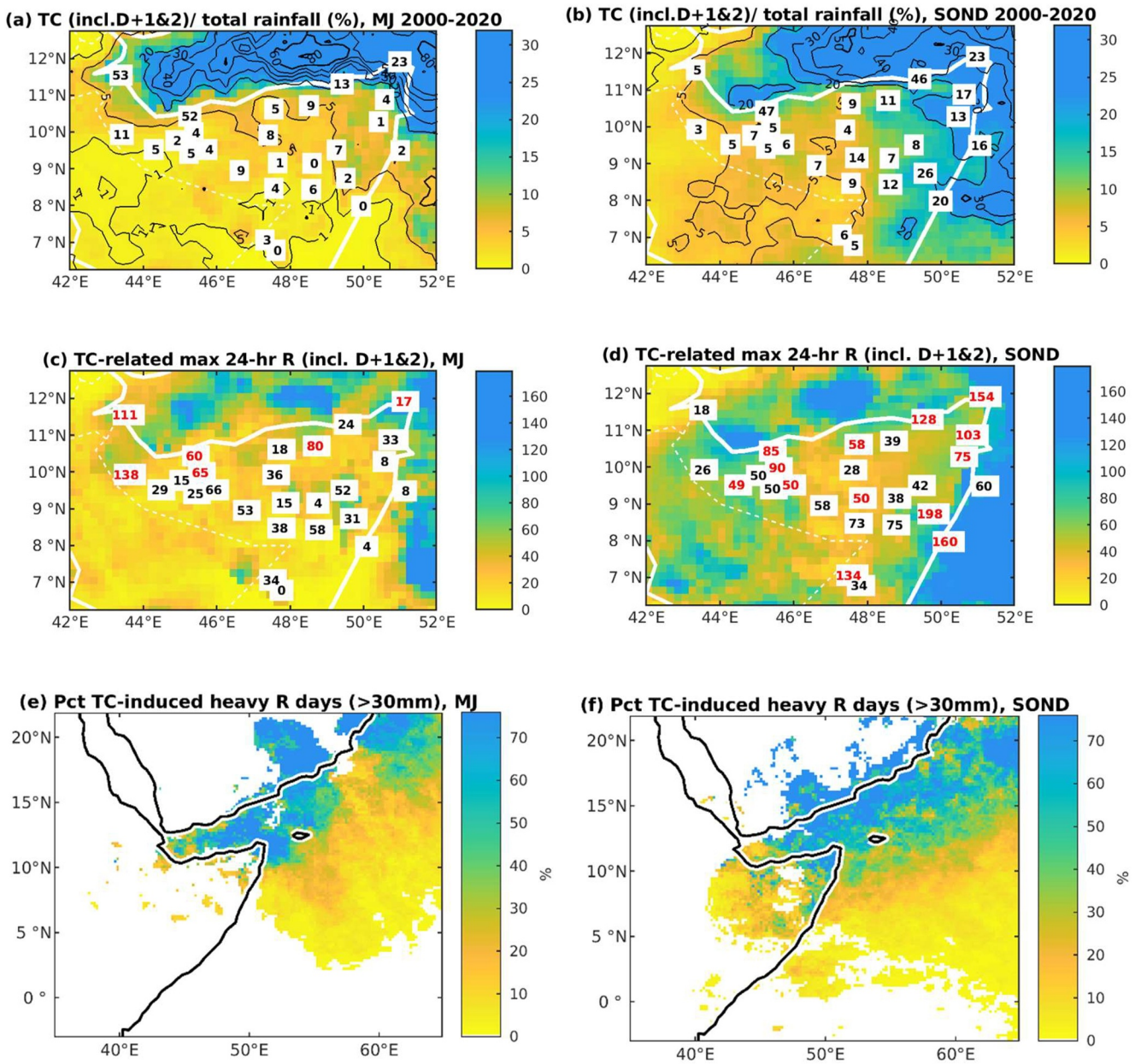

Figure 11. Rainfall statistics associated with tropical cyclones (TCs) over Northern Somalia, Djibouti and neighboring areas, based on rain-gauge data (figures) and IMERG (shadings), for May–June (MJ) (left panels) and September–December (SOND) (right panels). Percentage contribution of TC-related rainfall to mean seasonal rainfall (a, b); maximum TC-related 24-hr rainfall in mm (c, d); percent of days above 30 mm which are TC-induced (e, f), 2000–2020. In panels (c) and (d), a value in red indicates that it is the highest 24-hr amount recorded at a given station in the respective season. TC-related rainfall refers to rainfall within 750 km of the TC center, during its lifetime or in the two following days.

On the whole, despite the high expected variability associated with extreme point rainfall, relatively consistent patterns emerge in the northeastern Horn of Africa, which confirm the strong role of TCs on intense rainfall along the northern and eastern coasts in SOND, around the Gulf of Aden in MJ, as well as a substantial contribution inland but in SOND only.

3.4. Trends in Rainfall and TC-Related Rainfall

Annual rainfall trends are first analyzed over the period 2000–2020 (Figure 12a). For IMERG data, positive trends largely dominate, with the largest values (+5 to 10 mm/year) over inland Somalia and much of the WAS and

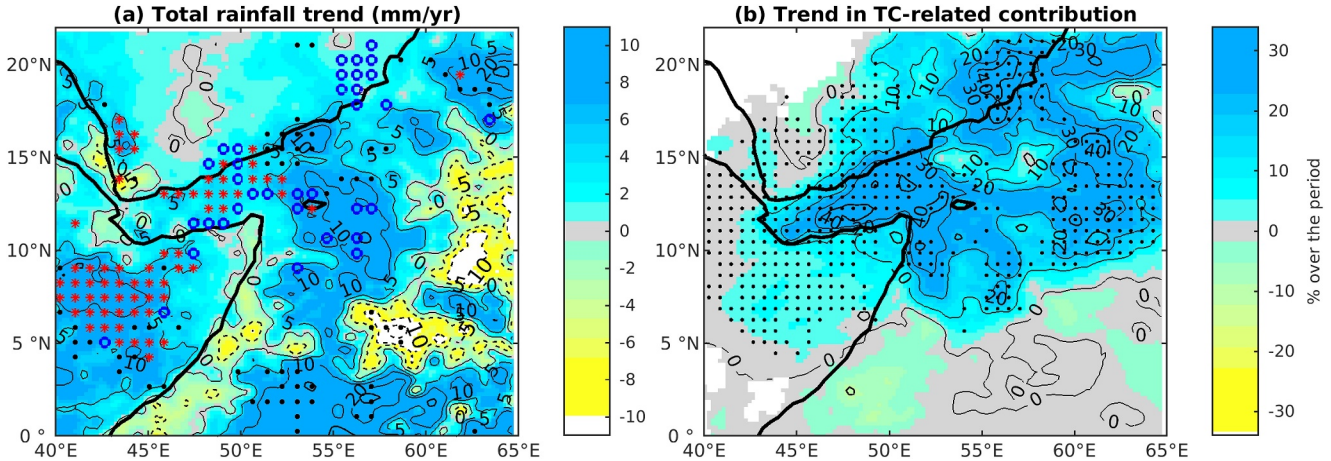

Figure 12. Annual rainfall trends, IMERG data, 2000–2020. Total rainfall (a), with symbols denoting significant trends ($p < 0.05$, Mann-Kendall test statistic). Blue circles: tropical cyclone (TC)-related rainfall; black dots: non-TC-related rainfall; red stars: significant trends in both TC-related and non-TC-related rainfall. Contribution of TC-related rainfall to the rainfall total (b). Dots indicate significant trends ($p < 0.05$).

Western Indian Ocean, although pockets of negative trends are found further offshore, notably around 5°N–60°E. There is some uncertainty about these negative trends, as PERSIANN data, over the same period, display positive trends even far offshore (not shown). The positive significant trends over parts of the Horn of Africa and the Gulf of Aden are generally due to an increase of both TC-related and non-TC-related rainfall (Figure 12a, red stars). Other parts of the Gulf of Aden and nearby grid-points to the east display positive significant trends in TC-related rainfall only (Figure 12a, blue circles), while more scattered grid-points exhibit a significant trend in non-TC-related rainfall only (black dots). The contribution of TCs to total rainfall shows significant positive trends over a large region covering the Gulf of Aden and neighboring areas (Djibouti, Yemen, northwestern Somalia), with a 21-year increase ranging from 20 to 35 points over the areas where the change is the largest, that is, part of the WAS, the coasts of Oman and Yemen, and the Gulf of Aden (Figure 12d). When removing TC-related rainfall from total amounts (Figure 12c), trends become close to zero or weakly positive in the northern part of the region, suggesting that much of the recent increased rainfall is due to the more frequent (and more intense) TCs. Over the African continent, apart from some coastal areas, there is little difference between the total and non-TC-related rainfall trends, despite the trend associated with TCs being significant, because TCs only contribute to a minor fraction of the rains.

A seasonal analysis (not shown) indicates that these trends are found during both MJ and SOND, although they are stronger and spatially more consistent for SOND. During this season, a very strong and significant ($p < 0.05$) increase in the TC contribution is noted between 10 and 17°N. In the 21-year period 2000–2020, the contribution of TCs to SOND rainfall amounts increased by 30%–50% in the Gulf of Aden and the Arabian Sea east of Socotra island. A similar rise is found from the Gulf of Aden to southern Oman in MJ, but it is more patchy and seldom significant, due to the rare occurrence of TCs in the pre-monsoon season, resulting in many years (even in the more recent period) with nil TC-related rainfall.

For a better appraisal of trends over the Gulf of Aden and its shores, a regional rainfall index (location shown on Figure 1) is extracted and plotted in Figure 13. For PERSIANN, the time-series were extended to include the full period from 1990 to 2020. Total rainfall shows a weak positive long-term trend (+0.44 mm/year from 1990 to 2020, i.e., +8% in 31 years). TCs strongly contribute to this trend, as shown by the conspicuous increase in TC-related rainfall (+0.67 mm/year Figure 13b). If one deducts TC-related rainfall from the annual rainfall, the trend becomes slightly negative (−0.23 mm/year, i.e., about −4% in 31 years). The contrast between the almost absence of any TC in the sub-period 1990–2007 and the relatively frequent TCs in the sub-period 2008–2020 is noteworthy. Besides the higher frequency of TCs, rainfall associated with each TC tends to significantly increase between 1990 and 2020 (Mann-Kendall tau, $p < 0.01$, not shown).

Over the period common to the two data sets, IMERG data show a relatively good agreement with PERSIANN in the interannual variations of total and TC-related rainfall. Over this period (2000–2020), the increase in TC-

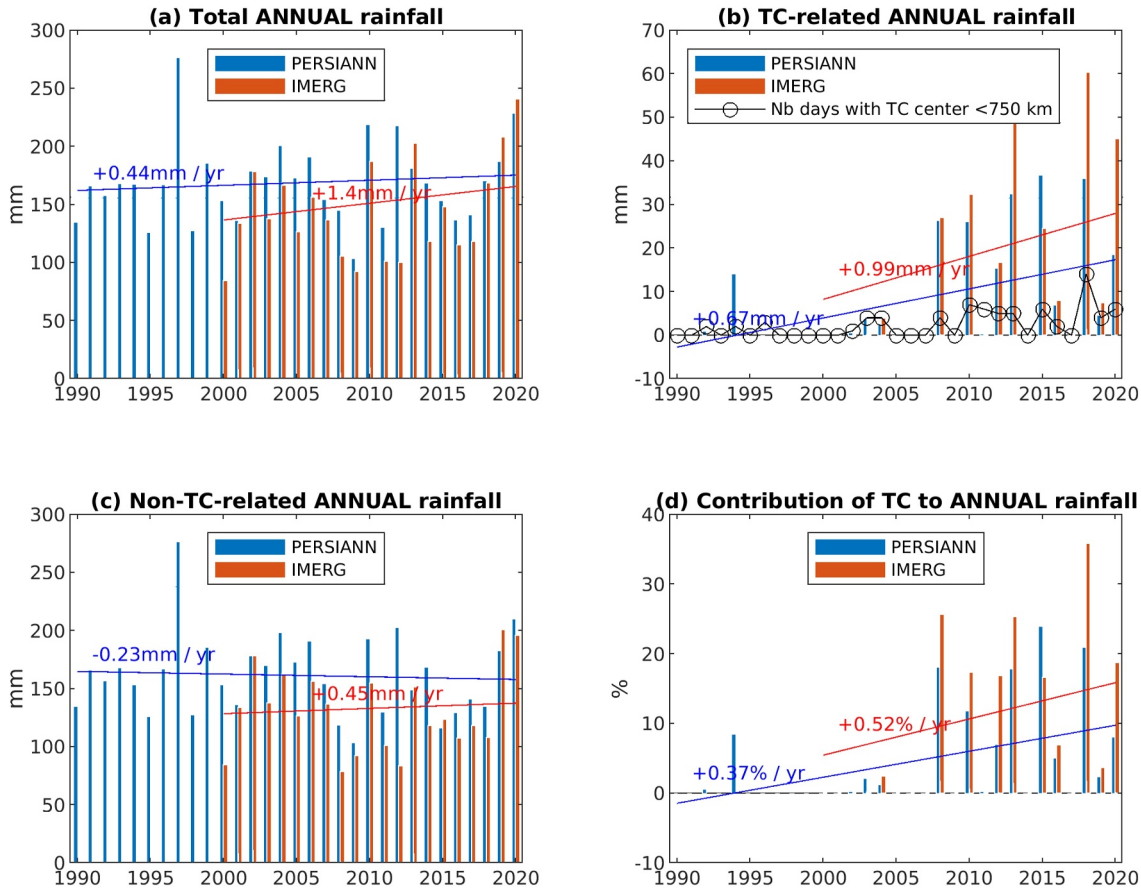

Figure 13. Annual rainfall variations and trends over the Gulf of Aden and its shores (44–50°E, 10–14°N): total rainfall (a), tropical cyclone (TC)-related rainfall (b), non-TC-related rainfall (c), and contribution of TCs to total rainfall (d).

related rains is strong (+0.99 mm/year in IMERG, Figure 13b). This trend also strongly contributes to the overall rainfall trend (+1.40 mm/year), while the non-TC-related trend is weaker. As described above, there is a marked increase in the contribution of TCs to total rainfall, which was close to zero before 2007 and reached 9.3% in 2008–2020.

The increase concerns both cyclonic seasons, although pre-monsoon TCs are still a rarity in the Gulf of Aden (Figure 14). The increase in TC-related rainfall boosts the May rainfall peak in the second sub-period, and strongly contributes to alleviate the decrease which would have otherwise been found in October–December. At that time, TCs have a strong effect on rainfall amounts in the arid environment of the Gulf of Aden. In the sub-period 2008–2020, the increase in the frequency of TCs makes the contribution of TCs to total October–December rainfall reach 32.4%, from 2.5% in 1990–2007. These statistics are based on a sufficient number of events to be meaningful: during this season, from 2008 to 2020, 17 TCs hit the Gulf of Aden or approached it (within the 750 km radius), as against only 4 in the previous sub-period.

The on-and-off TC activity in the Gulf of Aden (and the Arabian Sea in general) is a conspicuous feature (Figure 13). Roy Chowdhury et al. (2020) showed that the positive Indian Ocean Dipole (IOD) event that occurred in 2015 stimulated the development of the dual TCs Chapala and Megh in the WAS in October–November, through a warmer than normal western Indian Ocean and lower sea-level pressure. Similar conclusions were reached by Akhila et al. (2022), who studied cyclones Kyarr and Maha in 2019, a positive IOD year. However, Sattar and Cheung (2019) and Yuan and Cao (2013) got more ambiguous results on the systematic role of the IOD on Arabian Sea cyclones.

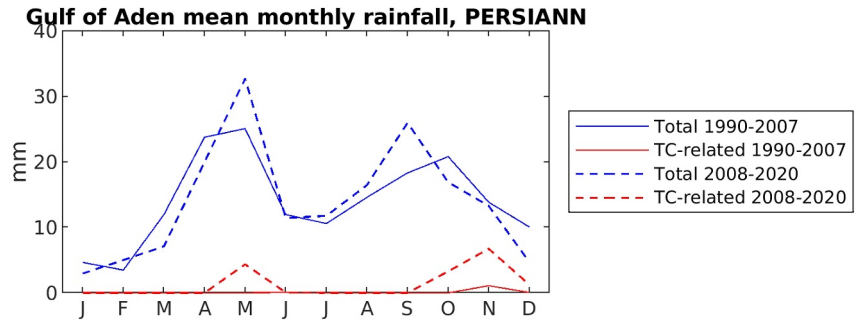

Figure 14. Mean monthly rainfall over the Gulf of Aden area (PERSIANN data; IMERG data not shown because of the small number of years available in the first sub-period), for 1990–2007 (solid lines) and 2008–2020 (dashed). Blue lines: total rainfall; red lines: tropical cyclone (TC)-related rainfall.

3.5. Regional Changes Contributing to the TC Increase

The changes in the oceanic and atmospheric conditions which may have accounted for the recent increase in the number of TCs or severe storms in the Arabian Sea have been partly documented by Deo et al. (2011), Deshpande et al. (2021), and Tiwari et al. (2022). This issue is further documented here, separately for the two cyclonic seasons, and by taking into account the detection of a change-point (in 2010) in the number of TC days in the WAS (Figure 2). Differences between the sub-periods 1990–2009 and 2010–2020 are plotted in Figure 15 using ERA5 reanalysis data (Hersbach et al., 2020; similar results are obtained using the NCEP-NCAR reanalysis).

The tripling of the number of days with TCs between 1990–2009 (4 days per year) and 2010–2020 (13 days per) in the WAS is found to be associated with three features favorable to TC activity:

(1) a decrease in vertical wind shear between 200 and 850 hPa in a belt running from India to the Gulf of Aden, though it is not significant over most of the domain, except the Gulf of Aden in SOND (Figures 15e and 15f)
(2) a sharp increase in relative humidity in the mid-troposphere (700–500 hPa, not shown) and of total column water (Figures 15c and 15d), mainly in the northwestern part of the region in MJ and in the eastern part in SOND
(3) an increase in SST (Figures 15a and 15b), which is more widespread in SOND than in MJ (for the latter, the Gulf of Aden and neighboring areas do not show any clear warming).

The main source region of TCs, that is, the southeastern Arabian Sea, displays the strongest sea surface warming, which may account for more favorable conditions for TC genesis, given that other factors in the same region (wind shear, atmospheric moisture) also tend to be more favorable. Over the WAS, it is the strong increase in total column water vapor, in MJ, and the reduced wind shear, in SOND, which seem to constitute the key triggers, likely enabling existing systems to have a longer lifetime or to intensify. The increased total column water also certainly contributes to the increase in the mean rainfall per TC as noted above for the Gulf of Aden.

Part of these changes denote the effect of decadal-scale variability, since pre-monsoon vertical wind shear over the WAS for the decade 2000–2009 was higher than in 1990–1999. This impacted the lower cyclone activity during part of the first sub-period. Deshpande et al. (2021) also pointed to an increase of TC genesis at lower latitudes, which due to the dominant easterlies across the Somalia and Yemen shorelines, contribute to the increased number of WAS cyclones during the most recent period (examples of 03A in November 2013, Sagar in 2018, Gati in 2020). Note that Figures 15e and 15f also display a meridional dipole in wind shear variations which is reminiscent of that found over the Bay of Bengal (Balaguru et al., 2016; Fan et al., 2019) and shown to be associated with changes in TC intensification rates and genesis location.

The trend in the WAS TC intensity (maximum sustained wind) is positive (+5 m/s from 1990 to 2020) but not significant. The same applies to the mean TC translation speed (−13% from 1990 to 2020). However, these features likely contributed to an increase in the rainfall amount associated with each TC, as depicted above for the Gulf of Aden. Geetha and Balachandran (2014) also documented a decrease in translation speed of cyclonic disturbances over the Arabian Sea during the decade 2001–2010 as compared with the earlier four decades, and at global scale decreasing translation speeds were shown to explain increased TC-related local rain rates

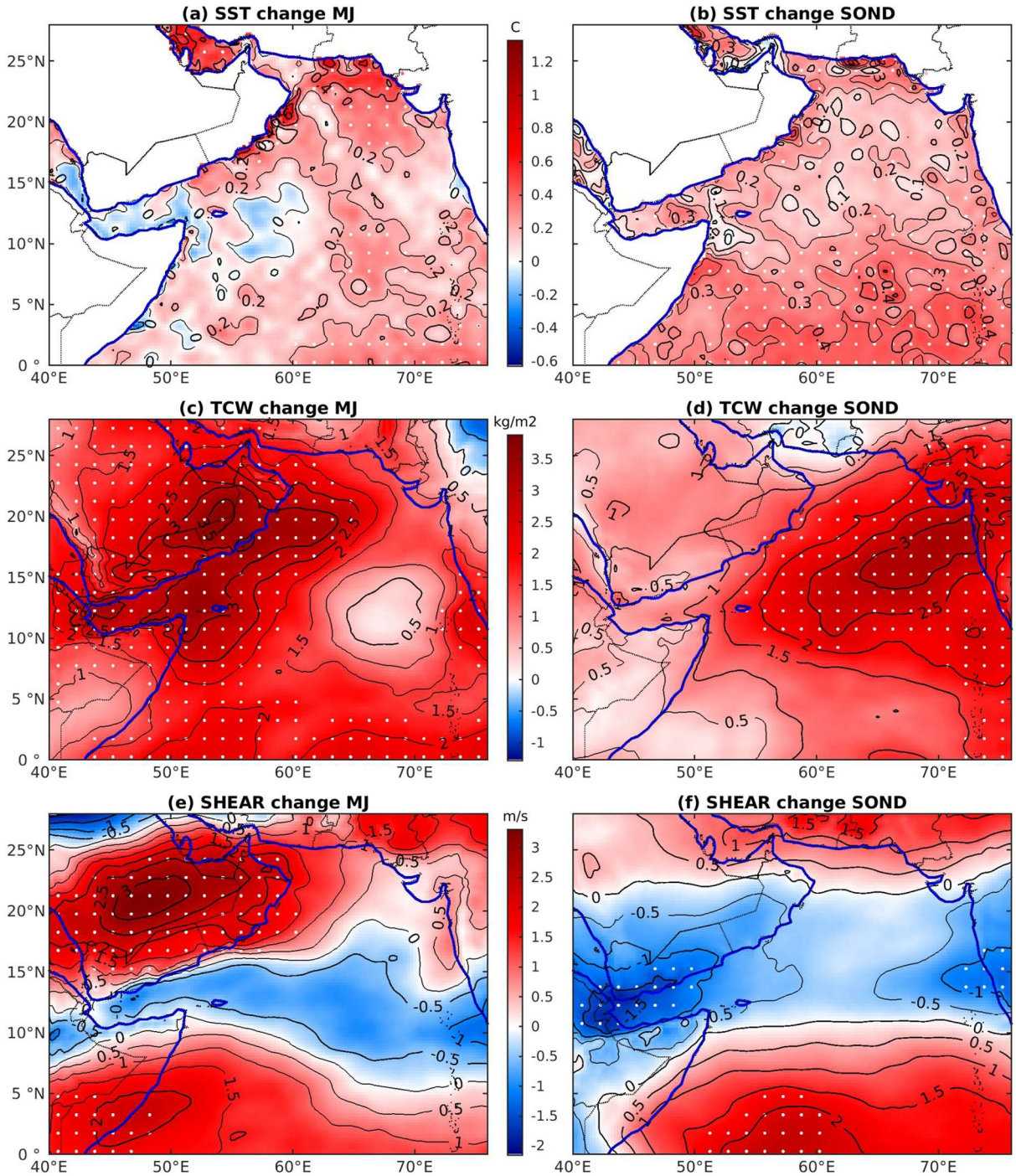

Figure 15. Changes in sea-surface temperature (a, b), total column water (c, d) and vertical wind shear (e, f) from 1990–2009 to 2010–2020, for the May–June (MJ) and September–December (SOND) seasons (ERA5 data). White dots indicate statistically significant changes (*t*-test, $p < 0.05$). The change in wind shear is computed as the magnitude change between 200 and 850 hPa wind vectors (Pillay & Fitchett, 2021).

(Kossin, 2018). It is unclear whether the WAS trends denote changes in TC activity due to anthropogenic climate change, but the Arabian Sea is one of the ocean basins where models most consistently project a forthcoming increase in intense TCs (Bell et al., 2020; Knutson et al., 2015; Murakami et al., 2013).

4. Conclusions

The northwestern Arabian Sea and adjacent land areas are among the few regions of the world where TCs occur in an arid context. Their contribution to rainfall and associated trends was analyzed using two combined satellite-rain-gauge precipitation products (PERSIANN and IMERG) and daily rain-gauge data for northern Somalia and Djibouti. Based on case studies and a statistical analysis of rainfall amounts with respect to the distance to the TC center, it was found that rainfall was influenced by TCs over a wide area (up to 750 km from the center), and that heavy rains still occurred one to 2 days after the TC lifecycle. Despite the rare occurrence of tropical systems (1.5 per year, whatever the category, with a third making landfall), they strongly contribute (30%–50%) to MAR over the northwestern Arabian Sea, Gulf of Aden and their respective coastlines. On a seasonal basis, this contribution is even higher (40%–60%) in southern Arabia and the adjacent oceanic areas, for both cyclonic seasons (May–June and September–December). High values were also found at the Gulf of Aden stations in Somalia in SOND. Over inland northern Somalia, contributions are lower in MJ (generally <5%) and SOND (5%–20%, increasing eastwards). In a belt running northeastward from the Gulf of Aden, a large proportion (30%–70%) of heavy rain days (>30 mm) are associated with TCs. In northern Somalia, many 24-hr maximum rainfall amounts are TC-related.

From 1990 to 2020, the number of tropical systems showed a marked increase in the region, hence their enhanced contribution to rainfall totals. Part of the overall upward rainfall trend over the northwestern Arabian Sea is actually the outcome of increasing cyclonic activity. Though over the Gulf of Aden and neighboring regions of the Horn of Africa (northern Somalia, Djibouti) TCs are very infrequent, the trend in TC-related rainfall shows a consistent and significant increase, highlighted by the contrast between the subperiods 1990–2007 and 2008–2020. Both cyclonic seasons are involved in this increase. The increase in TC frequency is related to a SST increase in the eastern and southern Arabian Sea, a decrease in vertical wind shear, and a strong increase in tropospheric moisture content.

Some caution should be exerted on the interpretation of these trends, which may not necessarily reflect the effect of anthropogenic climate change. Murakami et al. (2013) noted that, under increased greenhouse gases scenarios, a future westward shift of the mean locations of tropical storms is projected over the North Indian Ocean during the post-monsoon season (matching the recent increase in TC days in the WAS). Murakami et al. (2017) found that anthropogenic forcing has likely increased the probability of post-monsoon severe cyclonic storms over the Arabian Sea. S. Wang et al. (2023) likewise found a potentially dominant role of anthropogenic forcing on coastal TC frequency changes in many basins of the world, including the western coast of the Arabian Sea, but for the latter region their simulations failed to specifically attribute these changes to the effect of aerosol or greenhouse gases. Additionally, the low number of TCs in the early part of the period should also be considered in a broader context, since Rajeevan et al. (2013) showed a decrease in the frequency of intense TCs in the Arabian Sea from the period 1955–1973 to 1974–1992, suggesting large decadal-scale variability in the basin. Evan and Camargo (2011) questioned spurious increases in Arabian Sea TC intensity, which could explain part of the rise in cyclonic storm days they noted between 1979–1991 and 1992–2008 over the Arabian Sea as a whole. Duplicating this study for future periods is now needed, although this discussion highlights that internal climate variability cannot be neglected to obtain robust projections of TC activity, and their impacts on rainfall. Large ensembles from the CMIP6 (Eyring et al., 2016) or MENA-CORDEX (Bucchignani et al., 2015) modeling exercises could be used for that purpose.

Data Availability Statement

IBTrACS cyclone data are available from Knapp et al. (2018). IMERG rainfall estimates from NASA can be obtained from Huffman et al. (2019), and PERSIANN-CDR rainfall estimates, produced by the Center for Hydrometeorology and Remote Sensing (CHRS) at the University of California, Irvine (UCI), are available from Sorooshian et al. (2014). SWALIM rainfall data for Somalia are available from https://climseries.faoswalim.org. Djibouti rainfall data are available on request from Agence Nationale de la Météorologie de Djibouti (https://www.meteodjibouti.com/). ERA5 data produced by ECMWF are available through the Copernicus Climate Data Store (https://cds.climate.copernicus.eu/cdsapp#!/dataset/reanalysis-era5-pressure-levels?tab=overview).

Acknowledgments
This research work was partially supported by the ACE impact program of the World Bank and the French Embassy in Djibouti (FSPI Climat). The authors thank the National Meteorological Agency (ANM) of Djibouti for the provision of daily rainfall data for the Republic of Djibouti and SWALIM for northern Somalia. SWALIM is a project managed by FAO with funding from The European Union, The Swiss Agency for Development and Cooperation, The Italian Cooperation, DFID, USAID and the Government of France. Calculations were performed using HPC resources from DNUM CCUB (Centre de Calcul de l'Université de Bourgogne).

References

Abdalla, O., & Al-Abri, R. B. Y. (2011). Groundwater recharge in arid areas induced by tropical cyclones: Lessons learned from Gonu 2007 in Sultanate of Oman. *Environmental Earth Sciences*, *63*(2), 229–239. https://doi.org/10.1007/s12665-010-0688-y

Akhila, R. S., Kuttippurath, J., Rahul, R., & Chakraborty, A. (2022). Genesis and simultaneous occurrences of the super cyclone Kyarr and extremely severe cyclone Maha in the Arabian Sea in October 2019. *Natural Hazards*, *113*(2), 1133–1150. https://doi.org/10.1007/s11069-022-05340-9

Al-Manji, S., Mitchell, G., & Al Ruheili, A. (2021). Arabian Sea tropical cyclones: A spatio-temporal analysis in support of natural hazard risk appraisal in Oman. In R. S. Meena (Ed.), *Agrometeorology*. IntechOpen. https://doi.org/10.5772/intechopen.96961

Baburaj, P. P., Abhilash, S., Mohankumar, K., & Sahai, A. K. (2020). On the epochal variability in the frequency of cyclones during the pre-onset and onset phases of the monsoon over the North Indian Ocean. *Advances in Atmospheric Sciences*, *37*(6), 634–651. https://doi.org/10.1007/s00376-020-9070-5

Balaguru, K., Leung, L. R., Lu, J., & Foltz, G. R. (2016). A meridional dipole in premonsoon Bay of Bengal tropical cyclone activity induced by ENSO. *Journal of Geophysical Research: Atmospheres*, *121*(12), 6954–6968. https://doi.org/10.1002/2016jd024936

Bell, S. S., Chand, S. S., Tory, K. J., Ye, H., & Turville, C. (2020). North Indian Ocean tropical cyclone activity in CMIP5 experiments: Future projections using a model-independent detection and tracking scheme. *International Journal of Climatology*, *40*(15), 6492–6505. https://doi.org/10.1002/joc.6594

Breña-Naranjo, J. A., Pedroso-Acuña, A., Pozos-Estrada, O., Jiménez-López, S. A., & López-López, M. R. (2015). The contribution of tropical cyclones to rainfall in Mexico. *Physics and Chemistry of the Earth, Parts A/B/C*, *83–84*, 111–122. https://doi.org/10.1016/j.pce.2015.05.011

Bucchignani, E., Mercogliano, P., Rianna, G., & Panitz, H. J. (2015). Analysis of ERA-Interim-driven COSMO-CLM simulations over Middle East – North Africa domain at different spatial resolutions. *International Journal of Climatology*, *36*(9), 3346–3369. https://doi.org/10.1002/joc.4559

Chazée, L. (2017). *Patrimoine socio-économique et naturel de la région du Cap Gardafui* (p. 330). L'Harmattan.

Cherel, J. P., Omar Ali, B., Nour Ayeh, M., & Vinet, F. (2020). Activités cycloniques et nouveaux risques dans le golfe d'Aden. Exemple des impacts socio-économiques du cyclone Sagar sur Djibouti en mai 2018. *EchoGéo*, *51*. https://doi.org/10.4000/echogeo.18859

Deo, A. A., Ganer, D. W., & Nair, G. (2011). Tropical cyclone activity in global warming scenario. *Natural Hazards*, *59*(2), 771–786. https://doi.org/10.1007/s11069-011-9794-8

Deshpande, M., Singh, V. K., Ganadhi, M. K., Roxy, M. K., Emmanuel, R., & Kumar, U. (2021). Changing status of tropical cyclones over the north Indian Ocean. *Climate Dynamics*, *57*(11–12), 3545–3567. https://doi.org/10.1007/s00382-021-05880-z

Dvorak, V. F. (1984). Tropical cyclone intensity analysis using satellite data. NOAA Tech. Rep. NESDIS 11 (p. 47).

Englehart, P. J., & Douglas, A. V. (2001). The role of eastern North Pacific tropical storms in the rainfall climatology of western Mexico. *International Journal of Climatology*, *21*(11), 1357–1370. https://doi.org/10.1002/joc.637

Evan, A. T., & Camargo, S. J. (2011). A climatology of Arabian Sea cyclonic storms. *Journal of Climate*, *24*(1), 140–158. https://doi.org/10.1175/2010jcli3611.1

Evan, A. T., Kossin, J. P., Chung, C. E., & Ramanathan, V. (2021). Arabian Sea tropical cyclones intensified by emissions of black carbon and other aerosols. *Nature*, *479*, 94–97.

Eyring, V., Bony, S., Meehl, G. A., Senior, C. A., Stevens, B., Stouffer, R. J., & Taylor, K. E. (2016). Overview of the Coupled Model Intercomparison Project Phase 6 (CMIP6) experimental design and organization. *Geoscientific Model Development*, *9*(5), 1937–1958. https://doi.org/10.5194/gmd-9-1937-2016

Fan, K., Wang, X., Foltz, G. R., & Balaguru, K. (2019). Meridional oscillation in genesis location of tropical cyclones in the postmonsoon Bay of Bengal. *Climate Dynamics*, *53*(3–4), 2103–2118. https://doi.org/10.1007/s00382-019-04794-1

Finney, D. L., Marsham, J. H., Walker, D. P., Birch, C. E., Woodhams, B. J., Jackson, L. S., & Hardy, S. (2020). The effect of westerlies on East African rainfall and the associated role of tropical cyclones and the Madden–Julian Oscillation. *Quarterly Journal of the Royal Meteorological Society*, *146*(727), 647–664. https://doi.org/10.1002/qj.3698

Fors, J. R. (1977). Tropical cyclone Kathleen. NOAA Technical Memorandum NWS WR-114 (p. 29).

Gaona, M. F. R., Villarini, G., Zhang, W., & Vecchi, G. A. (2018). The added value of IMERG in characterizing rainfall in tropical cyclones. *Atmospheric Research*, *209*, 95–102. https://doi.org/10.1016/j.atmosres.2018.03.008

Geetha, B., & Balachandran, S. (2014). Decadal variations in translational speed of cyclonic disturbances over NIO. *Mausam*, *65*(1), 115–136.

Gray, W. M. (1968). Global view of the origin of tropical disturbances and storms. *Monthly Weather Review*, *96*(10), 669–700. https://doi.org/10.1175/1520-0493(1968)096<0669:gvotoo>2.0.co;2

Hersbach, H., Bell, B., Berrisford, P., Hirahara, S., Horányi, A., Muñoz-Sabater, J., et al. (2020). The ERA5 global reanalysis. *Quarterly Journal of the Royal Meteorological Society*, *146*(730), 1999–2049. https://doi.org/10.1002/qj.3803

Hoarau, K., Bernard, J., & Chalonge, L. (2012). Intense tropical cyclone activities in the northern Indian Ocean. *International Journal of Climatology*, *32*(13), 1935–1945. https://doi.org/10.1002/joc.2406

Huffman, G. J., Stocker, E. F., Bolvin, D. T., Nelkin, E. J., & Tan, J. (2019). GPM IMERG final precipitation l3 half hourly 0.1 degree × 0.1 degree v06, Greenbelt, MD, Goddard Earth sciences data and information services center (GES DISC) [Dataset]. https://doi.org/10.5067/GPM/IMERGDF/DAY/06

IFRC. (2013). International Federation of Red Cross and Red Crescent Disaster Relief Emergency Fund: Somalia Tropical Cyclone. Retrieved from https://reliefweb.int/report/somalia/somalia-tropical-cyclone-dref-operation-n-mdrso002-update-no-1

Jiang, H., & Zipser, E. J. (2010). Contribution of tropical cyclones to the global precipitation from eight seasons of TRMM data: Regional, seasonal, and interannual variations. *Journal of Climate*, *23*(6), 1526–1543. https://doi.org/10.1175/2009jcli3303.1

Kabir, R., Ritchie, E. A., & Stark, C. (2022). Tropical cyclone exposure in the North Indian Ocean. *Atmosphere*, *13*(9), 1421. https://doi.org/10.3390/atmos13091421

Kebacho, L. L. (2022). The role of tropical cyclones Idai and Kenneth in modulating rainfall performance of 2019 long rains over East Africa. *Pure and Applied Geophysics*, *179*(4), 1387–1401. https://doi.org/10.1007/s00024-022-02993-2

Khouakhi, A., Villarini, G., & Vecchi, G. A. (2017). Contribution of tropical cyclones to rainfall at the global scale. *Journal of Climate*, *30*(1), 359–372. https://doi.org/10.1175/jcli-d-16-0298.1

Knapp, K. R., Diamond, H. J., Kossin, J. P., Kruk, M. C., & Schreck, C. J. (2018). International Best Track Archive for Climate Stewardship (IBTrACS) Project, Version 4 [Dataset]. *NOAA National Centers for Environmental Information*. https://doi.org/10.25921/82ty-9e16

Knapp, K. R., Kruk, M. C., Levinson, D. H., Diamond, H. J., & Neumann, C. J. (2010). The International Best Track Archive for Climate Stewardship (IBTrACS): Unifying tropical cyclone best track data. *Bulletin of the American Meteorological Society*, *91*(3), 363–376. https://doi.org/10.1175/2009BAMS2755.1

Knutson, T. R., Sirutis, J. J., Zhao, M., Tuleya, R. E., Bender, M., Vecchi, G. A., et al. (2015). Global projections of intense tropical cyclone activity for the late twenty-first century from dynamical downscaling of CMIP5/RCP4.5 scenarios. *Journal of Climate*, *28*(18), 7203–7224. https://doi.org/10.1175/JCLI-D-15-0129.1

Kossin, J. P. (2018). A global slowdown of tropical-cyclone translation speed. *Nature*, *558*(7708), 104–107. https://doi.org/10.1038/s41586-018-0158-3

Kpanou, M., Laux, P., Brou, T., Vissin, E., Camberlin, P., & Roucou, P. (2021). Spatial patterns and trends of extreme rainfall over the southern coastal belt of West Africa. *Theoretical and Applied Climatology*, *143*(1–2), 473–487. https://doi.org/10.1007/s00704-020-03441-8

Lavender, S. L., & McBride, J. L. (2021). Global climatology of rainfall rates and lifetime accumulated rainfall in tropical cyclones: Influence of cyclone basin, cyclone intensity and cyclone size. *International Journal of Climatology*, *41*(Suppl. 1), E1217–E1235. https://doi.org/10.1002/joc.6763

Lvončík, S., Vahalík, P., Bongers, F., Peijnenburg, J., Hušková, K., van Rensburg, J. J., et al. (2020). Development of a population of *Boswellia elongata* Balf. F. in Homhil nature sanctuary, Socotra island (Yemen). *Rendiconti Lincei. Scienze Fisiche e Naturali*, *31*(3), 747–759. https://doi.org/10.1007/s12210-020-00936-4

Murakami, H., Sugi, M., & Kitoh, A. (2013). Future changes in tropical cyclone activity in the north Indian Ocean projected by high-resolution MRI-AGCMs. *Climate Dynamics*, *40*(7–8), 1949–1968. https://doi.org/10.1007/s00382-012-1407-z

Murakami, H., Vecchi, G. A., & Underwood, S. (2017). Increasing frequency of extremely severe cyclonic storms over the Arabian Sea. *Nature Climate Change*, *7*(12), 885–889. https://doi.org/10.1038/s41558-017-0008-6

Neumann, C. J. (2017). A global tropical cyclone climatology. In *WMO global guide to tropical cyclone forecasting* (pp. 28–62). Retrieved from https://cyclone.wmo.int/pdf/Global-Guide-to-Tropical-Cyclone-Forecasting.pdf

Ng, B., Walsh, K., & Lavender, S. (2014). The contribution of tropical cyclones to rainfall in northwest Australia. *International Journal of Climatology*, *35*(10), 2689–2697. https://doi.org/10.1002/joc.4148

OCHA Somalia. (2020). *Somalia, tropical cyclone Gati update #2. ReliefWeb*. UN Office for the Coordination of Humanitarian Affairs. 24 November 2020. Retrieved from https://reliefweb.int/report/somalia/ocha-somalia-tropical-cyclone-gati-update-2-24-november-2020

Owuor, A., & David McRae, H. (2022). The control of the desert locusts (*Schistocerca gregaria*) in Somalia during the upsurge between 2019 and 2021. *Outlooks on Pest Management*, *33*(6), 221–226. https://doi.org/10.1564/v33_aug_02

Pedgley, D. E. (1969). Cyclones along the Arabian coast. *Weather*, *24*(11), 456–470. https://doi.org/10.1002/j.1477-8696.1969.tb03121.x

Pettitt, A. N. (1979). A non-parametric approach to the change-point problem. *Journal of the Royal Statistical Society: Series C (Applied Statistics)*, *28*(2), 126–135. https://doi.org/10.2307/2346729

Pillay, M. T., & Fitchett, J. M. (2021). On the conditions of formation of Southern Hemisphere tropical cyclones. *Weather and Climate Extremes*, *34*, 100376. https://doi.org/10.1016/j.wace.2021.100376

Prat, O. P., & Nelson, B. R. (2013). Mapping the world's tropical cyclone rainfall contribution over land using the TRMM multi-satellite precipitation analysis. *Water Resources Research*, *49*(11), 7236–7254. https://doi.org/10.1002/wrcr.20527

Priya, P., Pattnaik, S., & Trivedi, D. (2022). Characteristics of the tropical cyclones over the North Indian Ocean Basins from the long-term datasets. *Meteorology and Atmospheric Physics*, *134*(4), 65. https://doi.org/10.1007/s00703-022-00904-7

Rajeevan, M., Srinivasan, J., Niranjan Kumar, K., Gnanaseelan, C., & Ali, M. M. (2013). On the epochal variation of intensity of tropical cyclones in the Arabian Sea. *Atmospheric Science Letters*, *14*(4), 249–255. https://doi.org/10.1002/asl2.447

Ramsay, H. (2017). *The global climatology of tropical cyclones*. Oxford Research Encyclopedia of Natural Hazard Science. Retrieved from https://oxfordre.com/naturalhazardscience/view/10.1093/acrefore/9780199389407.001.0001/acrefore-9780199389407-e-79

Ray-Choudhuri, S., Subramanyan, Y. H., & Chellappa, R. (1959). A climatological study of storms and depressions in the Arabian Sea. *Mausam*, *10*(3), 283–290. https://doi.org/10.54302/mausam.v10i3.4062

Résumé Mensuel du Temps. (1972). *Résumé mensuel du temps en Territoire Français des Afars et des Issas* (p. 14). Service de la Météorologie. Octobre 1972.

Roy Chowdhury, R., Prasanna Kumar, S., Narvekar, J., & Chakraborty, A. (2020). Back-to-back occurrence of tropical cyclones in the Arabian Sea during October–November 2015: Causes and responses. *Journal of Geophysical Research: Oceans*, *125*(6), e2019JC015836. https://doi.org/10.1029/2019jc015836

Salih, A. A., Baraibar, M., Mwangi, K. K., & Artan, G. (2020). Climate change and locust outbreak in East Africa. *Nature Climate Change*, *10*(7), 584–585. https://doi.org/10.1038/s41558-020-0835-8

Sattar, A. M., & Cheung, K. K. (2019). Comparison between the active tropical cyclone seasons over the Arabian Sea and Bay of Bengal. *International Journal of Climatology*, *39*(14), 5486–5502. https://doi.org/10.1002/joc.6167

Schreck, C. J., Knapp, K. R., & Kossin, J. P. (2014). The impact of best track discrepancies on Global Tropical Cyclone climatologies using IBTrACS. *Monthly Weather Review*, *142*(10), 3881–3899. https://doi.org/10.1175/mwr-d-14-00021.1

Shanko, D., & Camberlin, P. (1998). The effects of the Southwest Indian Ocean tropical cyclones on Ethiopian drought. *International Journal of Climatology*, *18*(12), 1373–1388. https://doi.org/10.1002/(sici)1097-0088(1998100)18:12<1373::aid-joc313>3.0.co;2-k

Singh, K., Panda, J., & Mohapatra, M. (2020). Robustness of best track data and associated cyclone activity over the North Indian Ocean region during and prior to satellite era. *Journal of Earth System Science*, *129*(1), 84. https://doi.org/10.1007/s12040-020-1344-x

Singh, V. K., & Roxy, M. K. (2022). A review of ocean-atmosphere interactions during tropical cyclones in the north Indian Ocean. *Earth-Science Reviews*, *226*, 103967. https://doi.org/10.1016/j.earscirev.2022.103967

Sorooshian, S., Hsu, K., Braithwaite, D., & Ashouri, H., & NOAA CDR Program. (2014). NOAA Climate Data Record (CDR) of Precipitation Estimation from Remotely Sensed Information using Artificial Neural Networks (PERSIANN-CDR), Version 1 Revision 1 [Dataset]. *NOAA National Centers for Environmental Information*. https://doi.org/10.7289/V51V5BWQ

Tiwari, G., Kumar, P., Javed, A., Mishra, A. K., & Routray, A. (2022). Assessing tropical cyclones characteristics over the Arabian Sea and Bay of Bengal in the recent decades. *Meteorology and Atmospheric Physics*, *134*(3), 44. https://doi.org/10.1007/s00703-022-00883-9

Wahiduzzaman, M., Cheung, K., Luo, J. J., Bhaskaran, P. K., Tang, S., & Yuan, C. (2022). Impact assessment of Indian Ocean Dipole on the North Indian Ocean tropical cyclone prediction using a Statistical model. *Climate Dynamics*, *58*(3–4), 1275–1292. https://doi.org/10.1007/s00382-021-05960-0

Wang, B., Xu, S., & Wu, L. (2012). Intensified Arabian Sea tropical storms. *Nature*, *489*(7416), E1–E2. https://doi.org/10.1038/nature11470

Wang, S., Murakami, H., & Cooke, W. F. (2023). Anthropogenic forcing changes coastal tropical cyclone frequency. *npj Climate and Atmospheric Science*, *6*(1), 187. https://doi.org/10.1038/s41612-023-00516-x

Yuan, J., & Cao, J. (2013). North Indian Ocean tropical cyclone activities influenced by the Indian Ocean Dipole mode. *Science China Earth Sciences*, *56*(5), 8s55–865. https://doi.org/10.1007/s11430-012-4559-0